Investigation of Supercritical Fluids for Use in Biomass Processing & Carbon Recycling

---

A Dissertation presented to

The Faculty of the Graduate School at
The University of Missouri-Columbia

In Partial Fulfillment
of the Requirements for the Degree

Doctor of Philosophy

---

by

Doug Hendry

Prof William A Jacoby, Dissertation Supervisor

May, 2012

The undersigned, appointed by the dean of the Graduate School, have examined the dissertation entitled

Investigation of Supercritical Fluids for Use in Biomass Processing & Carbon Recycling

Presented by Doug Hendry,

A candidate for the degree of Doctor of Philosophy,
and hereby certify that, in their opinion, it is worthy of acceptance.

_____
Professor William A Jacoby, Biological & Chemical Engineering

_____
Professor Stephen Lombardo, Chemical Engineering

_____
Professor Paul Chan, Chemical Engineering

_____
Professor Ali Bulent Koc, Agricultural Systems Management

ACKNOWLEDGEMENTS

First and foremost, I would like to thank my advisor, Dr. William Jacoby, for his expert guidance and continuous encouragement throughout the course of this study and in preparation of the thesis. I would like to acknowledge the encouragement, advice and support of Dr. Stephen Lombardo, Dr. Paul Chan, and Dr. Bulent Koc as members of the advisory committee.

I wish to thank Gordon Ellison of the Agricultural Engineering workshop for making reactors, separators, feeders, and many other parts and accessories required for this investigation. I would like to thank Lakdas Fernando for his expertise in Gas Chromatography. I would like to thank my colleagues and fellow graduate students Chandrasekar Venkitasamy, Andrew Miller, Nikolas Wilkinson, Malithi Wickramathilaka, and Reza Espanani for their help during experimental planning and execution. I would like to thank Rita Preckshot for proof reading and formatting this thesis.

Finally, I would like to thank my family for their support and encouragement throughout my entire academic career.

ABSTRACT

An apparatus was built in the Mizzou Carbon Recycling Center to explore the continuous thermochemical conversion of biomass and model compounds in supercritical water. The apparatus was used to investigate gasification or biomass and other organics in supercritical water to produce fuel gases. It proved to be superior to other designs in that the apparatus was capable of achieving both high gasification efficiencies and high gasification rates. The apparatus is also amenable other thermochemical conversion processes including SCW oxidation (combustion), hydrolysis in super and subcritical water, or combinations thereof.

The continuous supercritical water gasification apparatus is used to investigate glucose gasification in supercritical water at high temperatures and low residence times. A 2^3 full factorial experiment was performed to determine the effects of feed concentration, temperature, and residence time on glucose gasification. Glucose is a good representative of cellulosic biomass. Additionally, supercritical water gasification of ethanol and butanol as biomass model compounds was explored over a range of residence times from 0.7 to 34 s. Residence time was decreased until turbulence was achieved ($\tau \leq 1.2$ s). As fluid transitioned from laminar to turbulent flow, gasification rate was maximized while gasification efficiency was reduced. Gasification rates up to 107 g/L-s were observed; this is nearly an order of magnitude higher than previously reported. Arrhenius parameters were estimated to model the intrinsic kinetics of gasification of model compounds in supercritical water operating in plug flow without any transport limitations in the radial direction; this technique has never before been applied to supercritical water gasification.

Separations relevant to operation the continuous supercritical water gasification apparatus, and thus a biorefinery, are explored with the motivation to increase purity and energy density of gasification products. The separation of a supercritical mixture of nitrogen

and carbon dioxide is investigated at pressures from 10 to 31 MPa and temperatures of -5° and 23°C. Nitrogen is used as a model compound for valuable fuel gases (H_2, CH_4) produced during SCWG. Nitrogen mole fraction increases in the positive vertical direction near the top of the pressure vessel leading to an effective separation. The separation effectiveness is increased with increased pressure and decreased temperature. Preliminary experiments were also performed with additional binary systems: CO_2/H_2, CO_2/CH_4, and CO_2/Air, all of which behave similarly to the CO_2/N_2 system. This kind of high pressure separation has applications in continuous processing of pressurized gasification products, other biomass refinery operations, and in the natural gas industry.

Solid feeding is an important issue during biorefinery operation. One of the largest delays with the implementation of SCWG technology on a large scale is the lack a reliable feeding mechanism for a variety of biomass and waste feeds. A novel feeder was developed to meet this need and is detailed. Finally, a complete mass and energy balance is performed on the supercritical water gasification apparatus. The final energy balance results in an energy density of the products that is 4-10 times higher than the required energy input suggesting that supercritical water gasification is a viable process. The energy balance also presents opportunities for water and heat recycle for added energy balance advantages.

TABLE OF CONTENTS

LIST OF FIGURES

LIST OF TABLES

LIST OF ABBREVIATIONS AND SYMBOLS

Most of these abbreviations are defined in the text, but provided here for quick reference.

Symbol	Meaning
CRC	Carbon Recycling Center – Doug's Primary Lab
HEPS	High Pressure Equilibrium Phase Separator
SCF	Supercritical Fluid
SCW	Supercritical Water
SCWG	Supercritical Water Gasification
CH_aO_b	Representative Biomass Species on a One Carbon Basis
GE	Gasification Efficiency
CE	Carbon Efficiency
d[C]/dt	Gasification Rate
T_c	Critical Temperature
P_c	Critical Pressure
R	Gas Constant
GA	Green Algae
HW	Hog Waste
SS	Sweet Sorghum
TL	Turkey Litter
SD	Sawdust
CC	Corn Cob
RS	Rice Straw
GL	Glucose
L	Length
ID, OD	Inner, Outer Diameter
C	Concentration
T	Temperature
τ	Residence Time
k	Specific Reaction Rate
E_a	Activation Energy
A	Pre-exponential Factor
n	Reaction Order (also used to represent number of experimental replications)
EtOH	Ethanol
BuOH	Butanol
Re	Reynolds's Number
V	Average Fluid Velocity
ν	Kinematic Viscosity
μ	Dynamic Viscosity
ρ	Density
c_p	Specific heat
k	Thermal conductivity
h	Heat transfer coefficient
x	Mole Fraction in a Specific Phase
z	Overall Mole Fraction (also used to represent linear distance down the reactor)

1. Introduction & Background Information.

1.1 BIOMASS

Biomass is plant-derived organic matter and is our only renewable carbon resource. Biomass is available in abundance and is distributed more evenly than fossil fuels. Biomass is the fourth largest source of energy in the world provides 15% of world's primary energy consumption and as high as 38% of primary energy of developing countries (Saxena 2008). Biomass can be effectively processed to produce food and fuel and is CO_2 neutral. One disadvantage of biomass is that it is labor intensive for collection and currently has low commercial impact due to competition from other forms energy. Compared with other renewable resources, biomass is very flexible; it can be used as fuel for direct combustion, gasified, used in combined heat and power technologies, or biochemical conversions.

Biomass has the potential to provide a cost-effective and sustainable supply of energy, while aiding countries in meeting their greenhouse gas reduction targets. Biomass gasification for fuel gas production, as detailed in section 2, has been practiced for over 100 years, but has seen little commercial impact due to competition from other fuel sources and other energy forms. However, biomass does have significant economic potential provided that fossil fuel prices increase in the future as their reserves diminish. An important issue if biomass is to replace fossil fuels is whether we can grow sufficient biomass to substitute main energy sources such as crude oil. The world's annual biomass growth is 118×10^9 tons, when calculated as dry matter. The energy equivalent of oil fuel on a weight basis is 2.5 times higher than that of dry plant biomass. The present crude oil production of 3×10^9 tons per year is therefore equivalent to 7.5×10^9 tons of biomass, which is 6.4% of the annual biomass growth.

The National Renewable Energy Laboratory, Colorado reported the recent estimate of the biomass resources available in the United States. Table 1.1 shows the biomass availability

estimate for Missouri and the United States (Milbrandt 2005). According to this report, the nation produces a little less than half a billion tons per year, however more recently, the U.S. Department of Energy released the Billion-Ton Report (DOE 2011) detailing U.S. biomass feedstock potential. The report examines the nation's capacity to produce a billion dry tons of biomass resources annually for energy uses without impacting other vital U.S. farm and forest products, such as food, feed, and fiber crops. The widespread use of energy from *renewable* resources could address issues of concern today including greenhouse gas emissions, national energy security, air pollution, and energy efficiency.

Type of Biomass	**Missouri**	**United States**
Crop Residues	6007	157194
Forest residues	1840	56612
Primary Mill Residues	1036	77125
Secondary Mill residue	69	2615
Urban wood residue	613	30902
Municipal discards	273	12380
Switch grass on Conservation Reserve Program lands	8473	83572
Methane from manure management	120	2189
Methane from domestic wastewater	9	465
Total Biomass	18440	423054

Table 1.1. Estimated biomass availability in the US and Missouri (1000 tons per year).

1.2 SUPERCRITICAL FLUIDS AND THEIR USE IN BIOMASS PROCESSING

A supercritical fluid is any substance at a temperature and pressure above its critical point, where distinct liquid and gas phases do not exist. It can effuse through solids like a gas, and dissolve materials like a liquid. Figure 1.1 presents phase diagrams of a pure species, and shows the regions where supercritical conditions are achieved.

In the pressure-temperature phase diagram, Figure 1.1a, the lines between each phase indicate conditions where two phases exist in equilibrium. The line separating the liquid and vapor regions for example represents boiling and ends in the critical point, where the liquid and gas phases disappear to become a single supercritical phase. In the pressure-volume phase diagram, Figure 1.1b, the critical point is where the critical temperature isotherm has an

inflection point. From the P-V diagram, it can be seen that below the critical point temperature the isotherm shows discontinuity, but above the critical point the isotherm is continuous.

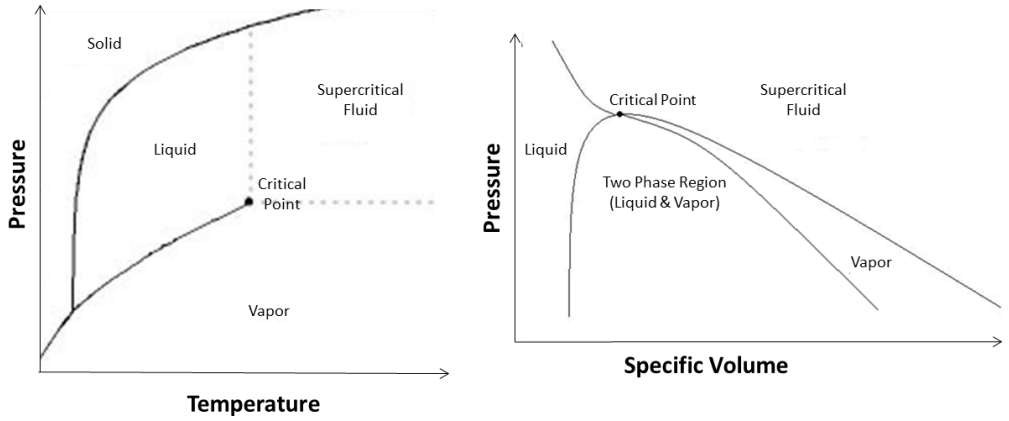

Figure 1.1. Phase diagram for a pure species on a P-T (a) and a P-V (b) diagram. The critical point and supercritical fluid region is identified.

The two most common applications of supercritical fluids in biomass processing are supercritical fluid extraction and supercritical fluid decomposition. The advantages of supercritical fluid extraction (compared with liquid extraction) are that it is relatively rapid because of the low viscosities and high diffusivities associated with supercritical fluids. The extraction can be selective to some extent by controlling the density of the medium and the extracted material is easily recovered by simply depressurizing, allowing the supercritical fluid to return to gas phase and evaporate leaving no solvent residues. Carbon dioxide is the most common supercritical solvent for extraction. It is used on a large scale for the decaffeination of green coffee beans, the extraction of hops for beer production, and the production of essential oils and pharmaceutical products from plants.

Supercritical water can be used to decompose biomass and other waste materials via supercritical water gasification. This type of biomass gasification can be used to produce hydrocarbon fuels for use in an efficient combustion device or to produce hydrogen for use in a fuel cell. Most of this report will focus on the development of the technology to convert and

separate low value biomass and other carbonaceous waste materials into higher value fuel gases.

1.3 SUPERCRITICAL WATER

The critical point of water is 22 MPa and 374°C. SCW is a gas like state that has liquid-like densities and gas-like viscosities. The thermal properties of water have very significant changes at and around the critical point. In no other solvent can the properties near or above the critical point be changed more strongly as a function of pressure and temperature than in water (Kruse 2008). Trends in properties variation in specific heat (c_p), thermal conductivity (k), heat transfer coefficient (h) and viscosity (μ) around the critical point are indicated in Figure 1.2. Here, $P > P_C$ and held constant while T is varied. The trends in Figure 1.2 are for water, but all pure species show similar tendencies around their respective critical point. Specific heat spikes around the critical point, but as temperature gets much above T_c, c_p returns to the same order of magnitude as subcritical water. The heat transfer coefficient, which quantifies the heat transfer by convection between the fluid and a solid, continues to increase even as temperature is much above T_c. Because of this, SCW is sometimes called a "high energy fluid" for its ability to quickly transfer heat to reactants during thermochemical reactions. A high heat transfer coefficient is one reason why SCW is so effective at decomposition of solid biomass at high temperatures. Thermal conductivity and viscosity both decrease when $T > T_c$. Thermal conductivity quantifies the fluid's ability to conduct heat within the fluid itself. Fluids with low viscosities make ideal solvents during chemical reactions because of their ability to encompass and penetrate the reactant. While not shown on Figure 1.2, there is no surface tension in SCW (or any other supercritical fluid).

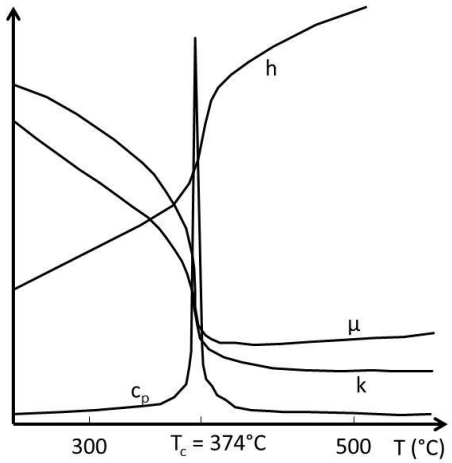

Figure 1.2. Variation in thermal properties around the critical temperature of water. Pressure is held constant ($P > P_c$).

The structure and properties of water change dramatically when its temperature rises. At the supercritical region, the high pressure keeps the density of the fluid close to those of liquids, increasing thermal conductivity (Boukis 2003). The high temperature keeps viscosity close to those observed in gases, increasing diffusion rates (Loppinet-Serani 2008). These combined properties of gases and liquids make SCW a good option as a solvent for many reactions. Table 1.2 summarizes the difference between ambient water and supercritical water in terms of several important characteristics.

When water is at supercritical conditions, the hydrogen bonds of water are weakened, and its dielectric constant decreases from about 78 at 25°C to the range 2 to 20 near the critical point, which is similar to that of polar organic solvents at room temperature. Water is an inexpensive and non-toxic solvent and reagent in its supercritical state. SCW has the ability to dissolve non-polar, organic compounds not normally soluble in liquid water or steam. This causes SCW to be able to dissolve many organic compounds completely, resulting in a single homogeneous phase, and making rapid reactions of organic compounds possible (Osada 2006; Yoshida 2003; Matsumura 2003).

Characteristics	Ambient Water	SCW
Dielectric Constant	78	<5
Solubility of Organics	Very Low	Fully Miscible
Solubility of Gases	Very Low	Fully Miscible
Solubility of Inorganics	Very High	Not Soluble
Diffusivity (cm^2/s)	$1x10^{5}$	$1x10^{-3}$
Viscosity (g/cm-s)	$1x10^{-2}$	$1x10^{-4}$
Density (g/cm^3)	1	0.2 - 0.9

Table 1.2. Characteristics of Water at Ambient and Supercritical Conditions

1.4 ENERGY CONVERSION TECHNOLOGIES FOR BIOMASS

A number of biochemical and thermochemical conversation technologies are used to process biomass to obtain valuable products from biomass. Biochemical conversion processes include anaerobic digestion, fermentation and oil extraction. These biochemical conversion processes are performed under conditions relatively close to ambient and occur much slower than thermochemical conversion processes. However, biochemical conversion processes are practiced reliably and profitably while most thermochemical conversion processes are not.

Thermochemical conversion processes include direct combustion, liquefaction, pyrolysis, and gasification. Direct combustion can be performed with many feedstocks including all kinds of lignocellulosic biomass to produce direct heat and energy. Hydrothermal liquefaction, which involves the application of heat and pressure to aqueous biomass, mimics the conversion of ancient plant material into the crude oil and natural gas reservoirs. In general, feedstocks containing ~80% water are subjected to subcritical temperatures to create a hydrophobic bio-oil with reduced oxygen content (10–18%) compared to the parent material (40%). Pyrolysis and gasification both occur without oxygen. Pyrolysis produces gas and liquid products and leaves a solid residue richer in carbon content called char. The process is used heavily in the chemical industry, for example, to produce charcoal, activated carbon, methanol, and other chemicals from wood or to convert biomass into syngas and biochar. Gasification is

performed at more extreme conditions than pyrolysis and thus more of the feed is converted into fuel gases rather than liquid and solids.

While there are several gasification plants around the world (Enerkem 2012), there are none that operate profitably. While not practiced commercially, the main advantage of gasification is that using the fuel gases produced are more efficient than direct combustion of the original feedstock because it can be combusted at higher temperatures or even in fuel cells. From a thermodynamic viewpoint, the upper limit to the efficiency defined by Carnot's rule is higher or not applicable. Figure 1.3 shows the typical operating condition ranges of various biomass conversion processes. An increase in the severity of each process causes an increase in the internal energy of the fluids and an increase in the rate of conversion. The internal energy of the fluid may also be used in subsequent processing to drive separations. A high rate of conversion and integrated separations reduce the capital and operating costs, as well as the size, of a plant for a given output.

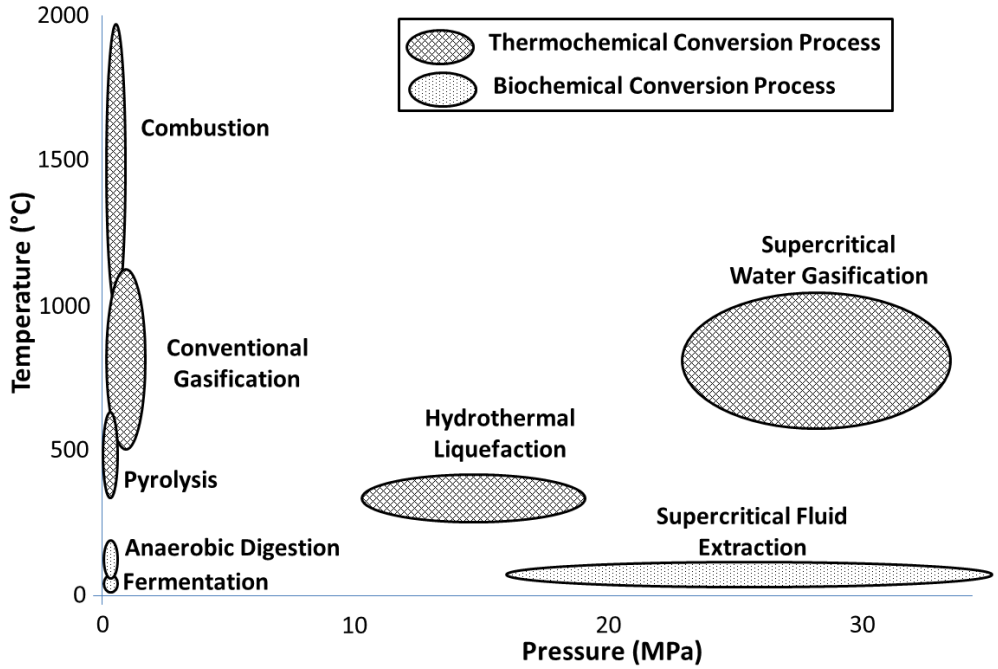

Figure 1.3. Comparison of process conditions of supercritical water gasification and other biomass conversion processes.

1.5 THERMODYNAMICS OF COMBUSTION & GASIFICATION

The two types of thermal decomposition reactions in which the main products are gases are combustion and gasification. Combustion takes place with excess oxygen. In this case, energy (heat) is obtained directly in one step. The exothermic reaction mechanism for combustion is below where CH_aO_b is a representative biomass on a one-carbon basis. Results from the CRC shows that typical heats of combustion (i.e. energy released when burned) for most biomass is 20 – 24 kJ/g (Venkitasamy 2011).

$$\mathrm{CH_aO_b} + \mathrm{O_2} \rightarrow \mathrm{CO_2}(v) + \mathrm{H_2O}(v)$$

Gasification is a technology that employs a reaction medium with oxygen content well below the stoichiometric requirement for combustion (i.e. essentially no oxygen). The endothermic reaction mechanism can be represented by the reaction below where CH_aO_b is a representative biomass on a one-carbon basis. Any sulfur, nitrogen, and phosphorus components of biomass are excluded for simplicity as they are known to end up in the liquid phase and we are most interested in the vapor fuel products.

$$\mathrm{CH_aO_b} + \mathrm{H_2O} \rightarrow \mathrm{H_2}(v) + \mathrm{CH_4}(v) + \mathrm{CO}(v) + \mathrm{CO_2}(v) + \mathrm{C_2H_6}(v)$$

While combustion releases energy, gasification is an endothermic process and creates energetic vapor products. Vapor products of thermal decomposition are simple. In combustion, the oxidation is substantially complete in one process, whereas gasification converts the intrinsic chemical energy of the carbon into a combustible gas of lighter compounds including H_2, CH_4, CO_2, and CO. Depending on the operating conditions and composition of the feed, the vapor product composition is typically in the following ranges: H_2: 25 – 40%, CH_4: 15 – 30%, CO: 1 – 10%, and CO_2: 25 – 40%. Results from the CRC show typical values for heat of gasification (i.e. energy required to gasify feed) for most biomass species is 2 – 4 kJ/g (Venkitasamy 2011). The vapor products of gasification can be standardized in terms of quality and is easier and more

versatile to use than biomass (McKendry 2002) in gas turbines, in fuel cells and for the synthesis of chemicals (Yoshida 2003). Combustion is commercially practiced (Bridgwater 2003; Faaij 2006) while gasification has not yet been made profitable anywhere in the world.

1.6 SUMMARY & RESEARCH OBJECTIVES

Several premises were developed to summarize the development and status of supercritical water gasification technology and direction of experiments detailed in this dissertation:

P_1: Biomass is our only renewable carbon resource.

P_2: Thermochemical conversion of biomass is a promising "end-of-pipe" technology for the biomass refinery.

P_3: Combustion of biomass is the only thermochemical conversion technology practiced profitably and reliably.

P_4: SCW is both a solvent and reactant in gasification reactions. It is cheap, nontoxic, ubiquitous, and recyclable.

P_5: Integration of biomass combustion and gasification can produce power and/or producer gas without energy input.

P_6: SCWG and combustion take a large variety of feed and convert to similar products.

P_7: To make SCWG technology economical and practical, continuous high throughput processing is needed.

P_8: Processing biomass in supercritical fluids gives opportunity for clean, efficient separations.

2. Literature Review.

2.1 SUPERCRITICAL WATER GASIFICATION

Biomass and other carbonaceous materials are converted into smaller molecules at high temperature. In the presence of oxygen, conventional combustion occurs forming CO_2 and water vapor and releasing energy. In the absence of oxygen, biomass gasifies in SCW to form mixtures of H_2, CH_4, CO_2, small amounts of CO, C_2H_6 and water vapor. Water can be removed from the permanent vapors in a high-pressure, equilibrium phase separator leaving a very dry (and valuable) mixture of H_2, CH_4, CO_2, and CO. This mixture has many potential uses mostly because of the high energy density of H_2 and CH_4 (Johnston 2005). On a mass basis, the high heating values of H_2 and CH_4 at ambient conditions are both higher than crude oil and coal. The process of SCW gasification produces the described valuable mixture of gases at high pressure, which also increases the volumetric energy density.

Water is present in all living biomass and dilutes the energy-density of harvested biomass. Removing water from biomass requires energy. Therefore, it makes sense to process biomass in water. Unlike conventional pyrolysis and gasification methods, supercritical water (SCW) can be used to gasify biomass without the expensive and energy-intensive step of drying the feedstock (Schmieder 2000).

Supercritical water gasification (SCWG) is superior to gasification in air because SCW is a good solvent that creates a homogeneous solution preventing charring. Supercritical water (SCW) is infinitely miscible in oxygen and air and is a good media for exothermic combustion. In the presence of oxygen, biomass undergoes a process called SCW Oxidation (SCWO). Bermejo and Cocero (2006) describe SCWO as well as its industrial development and applications. This characteristic highlights the potential for an integrated process in which the heat released by oxidation reactions is consumed by endothermic gasification reactions as proposed by Hong and

Spritzer (2002) among others. Modell (1978) described the conversion of solid or liquid organics to high energy gas in SCW with an energetically favorable reaction. Modell (1982) described a method to convert organic fuels or waste materials into useful energy for power generation and/or process heat. For most biomass, burning about one fourth to one third of the mass provides enough energy to gasify the remainder (Venkitasamy 2011). The literature reports in the sections below will summarize the developmental status of SCWG.

2.2 STUDIES OF BIOMASS GASIFICATION

The earliest and one of the key works on the supercritical water gasification was done by Modell (1977) on wood. The study was done on the effect of temperature and concentration of the gasification of glucose and maple sawdust in water in the vicinity of critical state at 374°C and 22 MPa. However, most of the research concerned with developing this technology into a commercialized process has only taken place recently. Several recent review articles summarize SCWG technology. Kumar (2009) provides a thorough review of the current status of biomass SCWG technology. Puig (2010) presents and analyses several gasification models based on thermodynamic equilibrium, kinetics and artificial neural networks. A series of different gasification process designs is presented by Ahrenfeldt (2011) with a focus on state-of-the-art processes with high reliability, flexibility and efficiency within cogeneration of energy commodities from conversion of biomass. Basu (2009) reviews the present state of the art and summarizes major observations arrived at in small scale laboratory flow and batch reactors. Perhaps the best recent review article on biomass gasification is by Kruse (2008), who performs a nearly exhaustive review of all related literature sources up to 2008. Guo (2010) reviews catalytic SCWG of biomass with a focus on hydrogen production. Catalysts have several advantages during SCWG, but complicate operations and may not be practical for implementation in an upscaled design. Catalysts may also be expensive and difficult to recover.

For these reasons, the use of catalysts in SCWG is undesirable and is not further investigated in this report.

Table 2.1 summarizes some novel, revolutionary reports of SCWG of biomass in a continuous flow reactor design. Only continuous designs are included because batch designs are not practical from an operational or commercialization prospective. Further, only designs with potential for upscale were included. However, for comparison, data from the CRC using a batch reactor is included at the end of the table. Gasification efficiency and rate are calculated in the same way for each report as described in section 3.2. The parameters in the table are either a range or represent one run: the run that led to the most innovative result. An innovative result would be one leading to high gasification rates, efficiencies, or best operation.

2.3 STUDIES OF GLUCOSE GASIFICATION

Glucose is a model compound for cellulose, which is the main constituent of biomass. Thus, glucose is often used as a model compound for studying biomass gasification. The main advantage to using glucose is that it is easy to pump and there is no sulfur, nitrogen, or phosphorus compounds leftover after conversion is complete. Matsumura (2005) performs a review of glucose gasification in SCW.

Table 2.2 summarizes the studies of glucose gasification in SCW reported in the literature, including results from our lab that are detailed in section 4.3. The table reports operating conditions (type of system, temperature, pressure, glucose feed concentration, residence time, presence or absence of catalysts), as well as gasification efficiency (GE), carbon efficiency (CE), H_2 yield to the extent as was reported in each study. Only one set of operating conditions is listed for each study. The conditions listed in the table are the conditions which achieved maximum rate of glucose gasification for each research group as described in the experimental section. In addition to the rate of glucose conversion, the table allows for direct

comparisons of GE, CE, and H_2 yield achieved by the different research groups at the given operating conditions. The methods used to calculate rate, GE, CE, and H_2 yield are described in the section 3.2 and were recalculated in the same way for each study for consistency.

2.4 GENERAL KNOWLEDGE ABOUT PROCESS VARIABLES IN SCWG

Examination of the results in Tables 2.1 and 2.2 as well as other literature sources reveals some general conclusions about effects of process variables in SCWG. Temperature is the process variable with perhaps the largest effect on gasification. Increasing temperature causes relatively large increases in gasification efficiency. It is seen in some studies that temperatures above 700°C are sufficient to gasify most biomass species, but require sufficiently long residence times to do so. Experiments from the CRC showed that increasing temperature from 750 - 800° at short residence times (4 s) caused an increase in gasification efficiency of 30% (Hendry 2011).

In addition to GE, temperature also has an effect on the vapor product composition, as shown in Figure 2.1. This figure was produced with results from Venkitasamy (2011), Lu (2007), Yan (2006), Yu (1993), and Tang (2005) using wood sawdust as a feed material. The figure was generated to show tendencies more than actual data because trendlines were smoothed to account for the fact that each reference collected data under slightly different concentrations and residence times. It is seen that increasing temperature increases H_2 yield and decreases CH_4 yield. This is primarily attributed to steam methane reforming (reverse methanation reaction) which is reversible but tends to favor H_2 at higher temperatures: $CH_4 + H_2O \rightarrow CO + 3\ H_2$. While CO is not a primary product or included in Figure 2.1 (its concentration is about an order of magnitude less than H_2), it shows an increase up until about 600°C.

Title	Lead Author	Year	Type of System	Feed Stock	Temperature	Pressure	Residence Time	Conc	Catalyst	Gasification Rate	Max GE	Notes
Exploration of the gasification of Spirulina algae in supercritical water	Miller	2012	Continuous	Algae	550 - 650°C	25 MPa	1 - 40 s	50 wt%	No	53 g/L-s	95%	Developed a fluid power feeder to pump algae slurries as low as 50% moisture and capable of overcoming transport limitations associated with laminar flow.
Biomass Gasification in Supercritical Water	Antal	2000	Continuous	Corn, Potato, Wood	650°C	22 MPa	Not Reported	15 wt%	No	3 g/l-s	100% GE (57% H_2 Yield)	Corn- and potato-starch gels, wood sawdust suspended in a cornstarch gel, and potato wastes were delivered to three different tubular flow reactors by means of a "cement" pump.
Biomass gasification in near- and super-critical water: Status and prospects	Matsumura	2005	Continuous	Cabbage	600 - 725°C	5 - 45 MPa	1 - 5 min (30 min Pre-treatment)	5 - 18 wt%	Yes (metal & alkali)	8 g/L-s	96%	Successfully applied a hydrothermal pre-treatment (150 - 200°C for feeding cabbage. Hemicellulose was dissolved and the cell structure of thebiomass was destroyed.
Evaluation of supercritical water gasificationand biomethanation for wet biomass utilization in Japan	Matsumura	2003	Continuous	Hyacinth	600°C	34.5 MPa	Not Reported	1 - 3 wt%	No	Small		Concluded that liquefaction before feeding or the use of dissolved feedstock by biochemical treatment makes pumping easier for wet biomass slurries.
Thermodynamic modeling and analysis of biomass gasification for hydrogen production in supercritical water	Lu	2006	Continous	Multiple	500 - 800°C	25 MPa	Not Reported	5 - 30 wt%	No	Not Reported	80%	Completed analysis of energy requirements and balance to incorporate a recycle water stream for increased pumping and energy efficiency.
Investigation of thermochemical conversion of biomass in supercritical water using a batch reactor	Venktasamy	2011	Batch	Algae, Corn, Rice Straw, Others	600 - 700°C	45 MPa	5 - 10 min	12 - 20 wt%	No	1 g/L-s	85%	Concluded the oxidation state of carbon atom of biomass is a key variable in determining the changes in enthalpy during both conventional combustion and supercritical water gasification.
Gasification of alcohols and algae in a supercritical water batch reactor: parameterization of rate expressions	Venktasamy	2012	Batch	Algae	700°C	45 MPa	100 - 120 s	20 wt%	No	1 g/L-s	60%	Was able to gasify algae as well as determine the reaction order and the parameters for an Arrhenius-type expression describing the temperature dependence of the rate constant.

Table 2.1. Summarization of published studies on biomass gasification in SCW in a continuous reactor with innovative feeding designs and novel results.

Title	Author	Year	Type of System	Temperature	Pressure	Residence Time	Conc	Catalyst	Rate (g/L-s)	Max GE/CE Yield	Max H_2 Yield
Exploration of the Effect of Process Variables on the Production of High-value Fuel Gas from Glucose via Supercritical Water	Hendry	2009	Continuous	750°C	34.5 MPa (5000 psi)	12 s	20 wt% (1.4 M)	No	22 g/L-s	114% GE, 105% CE	56%
Influence of phenol on glucose degradation during supercriticalwatergasification	Weiss	2011	Continuous	550°C	25 MPa	60 s	2 wt% (.1 M)	Yes (phenol, $KHCO_3$)	<1 g/L-s	<50%	<10%
Carbon-Catalyzed Gasification of Organic Feedstocks in Supercritical Water	Xu	1996	Continuous	600°C	34.5 MPa (5000 psi)	34 s	1.2M glucose (17.8 wt%)	Yes	6.54 g/L-s	103% CE	37%
Hydrogen Production by Steam Reforming Glucose in Supercritical Water	Yu	1993	Batch (Capillary Tube)	600°C	34.5 MPa (5000 psi)	30 s	.8 M glucose	No	4.27 g/L-s	89% CE	None reported
Gasification of Glucose in Supercritical Water	Lee	2002	Continuous Tubular Reactor	750°C	28 MPa (4000 psi)	19 s	.6 M glucose	No	5.67 g/L-s	GE 99.7% CE	80%
Hydrogen production from glucose used as a model compound of biomass gasified in supercritical water	Hao	2003	Continuous	650°C	25 MPa (3625 psi)	3.8 min (228 s)	.8 M glucose	No	.61 g/L-s	96.8% GE	84%
Hydrogen production by biomass gasification in supercritica lwater: A parametric study	Hao	2005	Continuous	650°C	25 MPa (3625 psi)	2.9 min (174 s)	0.2 M glucose	No	.18 g/L-s	111.4% GE 86.3% CE	90%
Gasification of Model Compounds and Wood in Hot Compressed Water	Kersten	2006	Batch (quartz capillaries)	700°C	300 bar (30 MPa, 4350 psi)	60 s	17 wt% (1.1 M) glucose	No	2.74 g/L-s	83% CE	18%
Reactor Development for Supercritical Water Gasification of 4.9 wt% Glucose Solution at 673	Yoshida	2009	Continuous	400°C	25.4 MPa (3680 psi)	37 s	4.9 wt% (.3M) glucose	No	1.37 g/L-s	94% CE	36%
Partial Oxidative and Catalytic Biomass Gasification in Supercritical Water: A Promising	Yoshida	2004	Continuous	400°C	25.7 MPa (3700 psi)	1 min (60 s)	4000 ppm (.22 M glucose)	Yes (see note)	.63 g/L-s	96% CE	39%
Catalytic hydrogen generation from biomass (glucose and cellulose) with ZrO2 in supercritical water	Watanabe	2002	Batch	440°C	Not specified	10 min (600 s)	1.4 M glucose	Yes (zirconia)	N/A	Not specified	5%
Influence of the Heating Rate and the Type of Catalyst on the Formation of Key Intermediates and on the Generation of Gases During Hydropyrolysis of Glucose in Supercritical Water in a Batch	Kruse	2004	Batch	500°C	Not specified	1 hour (3600 s)	5 wt% (.3 M glucose)	Yes	N/A	Not specified	32%

Table 2.2. Summarization of published studies on glucose gasification in SCW.

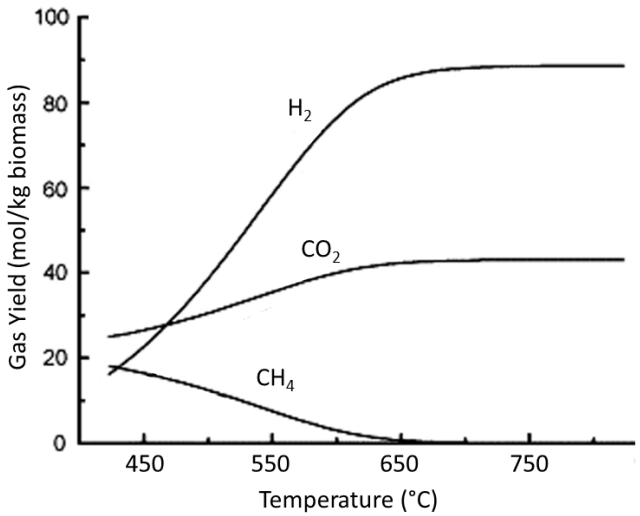

Figure 2.1. Gas yield of H_2, CH_4, and CO_2 as a function of temperature for SCWG of sawdust.

While temperature has a large effect on SCWG on SCWG of biomass, pressure is known to have a negligible effect. Changes in pressure in the range of 22–33 MPa do not have an effect on SCW gasification (Hendry 2011, Venkitasamy 2011, Kersten 2006). Because pressure does not affect gasification, changing pressure in this range can be used to operationally change the density of the reacting fluid and the residence time in continuous processes. Several studies from our lab estimate the effect of residence times on SCWG. Increasing residence time from 4 to 6.5 s increased gasification efficiency by 9% while decreasing gasification rate by 9 g/L-s (Hendry 2011). During SCWG of algae, increasing residence time from 4 to 9 s increased gasification efficiency by 20% (Miller 2012).

Concentration is known to affect SCWG of biomass. In batch processes, the concentration is often referred to as biomass loading. Holding other variables constant, increasing concentration will decrease the gasification efficiency, but increase the gasification rate (Hendry 2011, Miller 2012, Kruse 2008). Results from our lab show that increasing concentration from 10% to 15% at high temperature and low residence times reduced gasification efficiency by 30%, but increased gasification rate by 3 g/L-s (Hendry 2011 and see section 4.3 below). Further results showed that increasing concentration from 17.5% to 25% at

moderate temperatures and low residence times reduced gasification efficiency of algae by 9.4% (Miller 2012). Figure 2.2 below estimates the effect of concentration (loading) on vapor product composition. This figure was produced with results from Venkitasamy (2011), Yoshida (2003), Lu (2007), and Yan (2006), using wood sawdust as a feed material. As with Figure 2.1 above, Figure 2.2 was generated to show trends more than actual data because trendlines were smoothed and each reference collected data under different temperatures and residence times.

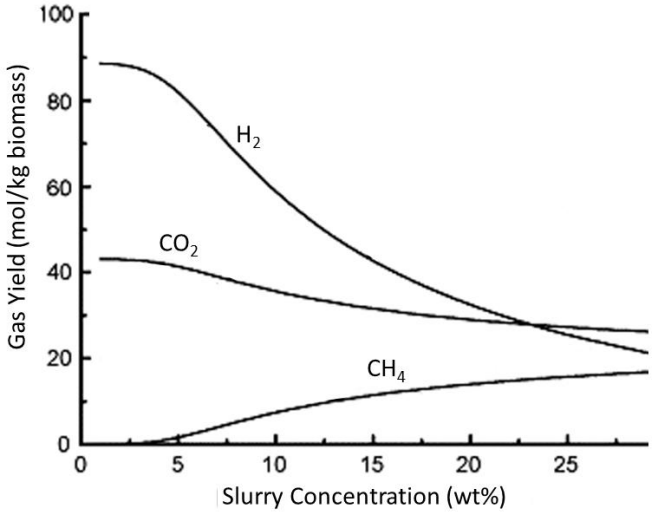

Figure 2.2. Gas yield of H_2, CH_4, and CO_2 as a function of biomass loading wood sawdust.

Besides temperature, concentration, and residence time, the variable that has the largest effect on SCWG of biomass is the composition of the feed. One way to quantitatively represent the composition is with the average oxidation state of a carbon atom in the feed (Venkitasamy 2011). The SCWG mole fractions of H_2, CO_2 and CH_4 produced during the experiments of 8 biomass species in the CRC are plotted against the oxidation state of carbon atom in the samples in Figure 2.3. In Figure 2.3, the dependent variable is the composition of the eight samples. The labels of each species, from left to right are: green algae, hog waste, sweet sorghum, turkey litter, sawdust, corn cob, rice straw, and glucose. The mole fraction of CO_2 and CH_4 correlate well with the oxidation state of the carbon atom (R^2 = 0.96 for both). The mole fraction of CO_2 increased with the oxidation state of carbon, at the expense of mole

fraction of CH_4. The mole fraction of hydrogen did not correlate with the oxidation state of the carbon atom, as H_2 is formed from several different mechanisms besides direct gasification including the splitting of water and from water gas shift: $CO + H_2O \rightarrow CO_2 + H_2$.

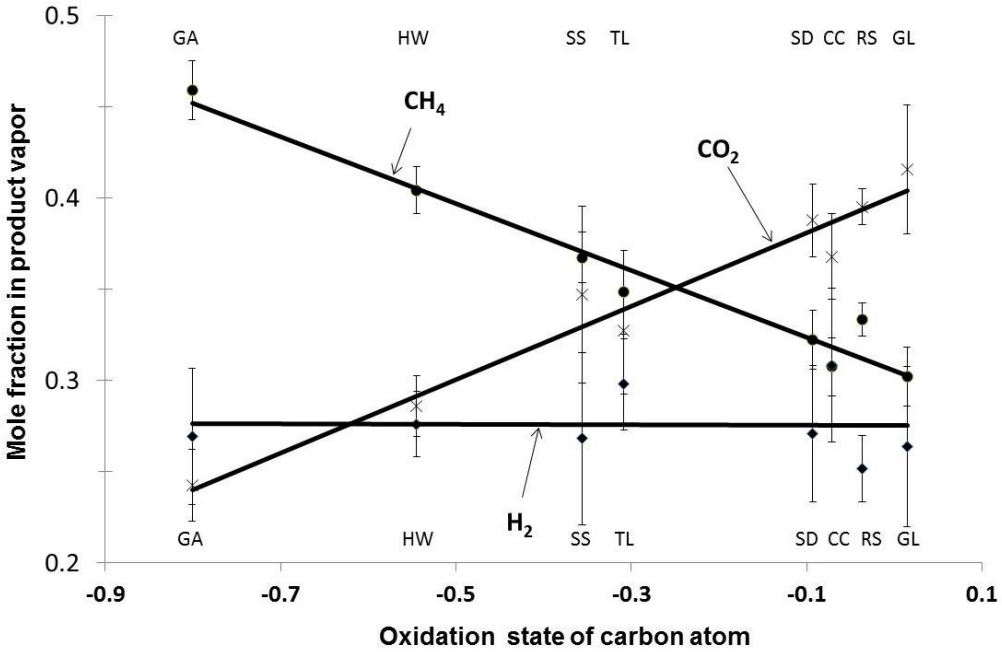

Figure 2.3. Effect of feed composition (represented by the average oxidation state of a carbon atom) on composition of vapor product of SCWG of 8 biomass feeds.

2.5 ANALYSIS OF LIQUID PHASE AND SOLID RESIDUE

The analysis of the liquid phase and solid residues is much less important in SCWG than in other thermochemical and biochemical conversion processes (see Figure 1.3 in section 1.4) because fuel gas is the primary and most valuable product of SCWG. Further, in a practical SCWG process, the gasification efficiency should be close to 1, so unconverted feed is much less dominant than the vapor phase. Thus, analysis of the liquid phase is not the focus of the experiments presented in this report. Nevertheless, the composition of the liquid phase is important to complete mass and energy balances and explore the uses of this phase.

The main intermediates in the water soluble fraction of SCWG were analyzed. There were many intermediates in the SCWG of sawdust and cellulose including acetic acid, formic

acid and glycolic acid, aldehydes (acetaldehyde, formaldehyde), phenol and phenol derivatives, furfural, methyl furfural, hydroxymethyl furfural (Sinag 2009, Savage 1999, Yoshida 2001). However, at high temperatures (> 650°C) and fast heating rates, the amount of acids and other toxic compounds appears to be small in favor of products like sugars often seen in hydrolysis processes (Sinag 2009, Guo 2010, Puig 2010). Any solid phase not soluble in the liquid phase is primarily unconverted carbon (Sinag 2009). However, this phase is very small because the carbon efficiencies of most practical processes are close to 100%. Any nitrogen in the biomass feed almost entirely ends up in the liquid phase as ammonia. Any sulfur also almost entirely ends up in the liquid phase as sulfates. Likewise, any phosphorus appears as phosphates in the liquid phase (Guo 2010, Puig 2010). The fate of nitrogen, sulfur, and phosphorus indicates that the liquid phase may be a good fertilizer, provided gasification temperatures are high enough to reduce the amount of acids to acceptable levels.

2.6 REVIEW OF REACTOR DESIGNS

Throughout the literature, there are several types of reactors used to study SCWG of biomass. The most prevalent is the batch reactor. In the laboratory, the use of a batch reactor has many advantages. Batch reactors are simple, inexpensive, and easy to operate. Virtually any carbonaceous sample can be charged. The biggest disadvantages of a batch reactor relative to a continuous reactor is a much slower heating rate which is known to negatively affect gasification as hot water chemistry such as polymerization or charring can reduce gas yield in a batch reactor (Venkitasamy 2011).

While batch reactors can be useful on a laboratory scale, large-scale conversion of biomass and residues must be undertaken on a continuous basis. To obtain equal performance, the residence time of a continuous reactor is orders of magnitude less than a batch reactor. This allows for a very high throughput design. In a well-designed continuous reactor with a preheat

stream, the biomass slurry can be heated nearly instantaneously to a supercritical state (Hendry 2011). See Figure 3.1 in section 3.1 below for a schematic of the continuous SCWG apparatus in the CRC as an example of a well-designed continuous reactor. If the continuous reactor does not have a preheat stream, it often suffers the same hot water chemistry problems as a batch reactor.

While a continuous reactor is clearly advantageous for high throughput SCWG processes, all of the reports available on continuous SCWG reactors operate in laminar flow. In some chemical conversion processes, it is known that turbulent flow enhances mixing and thus conversion efficiency. The continuous apparatus in the CRC is the only reported SCWG reactor capable of operating in turbulent flow, thus eliminating axial gradients in temperature and concentration. Results from our lab show that achieving turbulent flow leads to the highest gasification rates but not gasification efficiencies (Hendry 2012; Miller 2012). See Figure 5.2 in section 5.5 for more detail on the effect of flow on SCWG.

Thus far, no reactor has proved capable of combining high gasification rates and high gasification efficiencies during SCWG under the same conditions. However, results from the CRC give insight into upscale reactor designs. Such reactors will have dimensions such that L>>D. Reactor lengths (L) must be appropriately large so that the reacting fluid is heated for sufficient residence times for high gasification efficiencies. Reactor diameters (D) must be small enough to remove concentration variation across the diameter (turbulent flow and high Reynolds numbers) so that high gasification rates are achieved. However, reactor diameters must be several times larger than the particle size to avoid char buildup and clogging.

3. Construction of Continuous SCWG Apparatus and Research Methods.

As mentioned above, an apparatus was built in the CRC to explore the continuous thermochemical conversion of biomass and model compounds in supercritical water. Most of the research done using the apparatus involved gasification in supercritical water to produce fuel gases. However, the apparatus is also amenable other thermochemical conversion processes including SCW oxidation (combustion), hydrolysis in super and subcritical water, or combinations thereof. These processes are detailed in sections 1.4 and 1.5.

3.1 ORIGINAL CONTINUOUS REACTOR APPARATUS DESCRIPTION

Figure 3.1 shows the schematic of the original SCW continuous reactor apparatus. Several significant modifications have been made to the original apparatus and will be detailed below. The reactor is constructed from a 60 cm length of 316 stainless steel tubing. Several differently sized reactors were used. Reactors of different inner diameter effect the residence time and hydrodynamics of the reacting fluid. Specific reactor sizes are specified with each set of experiments described in the experimental section. Reactors were made in-house by Gordon Ellison, a machinist in the Agricultural and Biological Engineering Departments. The rest of the system is plumbed using 316 stainless steel tubing (0.64 cm OD, 0.21 cm ID). The apparatus is rated at 140 MPa at ambient temperatures. At elevated temperatures, the pressure rating is reduced but the system proved capable of operating up to 40 MPa.

Stainless steel is perhaps the best material to use for SCWG because it does not exhibit any corrosion during SCWG when catalysts are not used. Some reports (Kruse 2008; Guo 2010) report slight corrosion when using relatively high concentrations of alkali salts as catalysts. However at high temperatures, catalysts do not increase gasification and are undesirable operationally, so there is not expected to be any corrosion of the reactor. It should be noted that the preheat stream does need to be replaced at regular intervals (about every 200 hours)

because it is susceptible to bursting. The bursting is due to the relatively cool water flowing into the hot tubing and weakening the steel over time.

Several different feeding mechanisms were used with successive generations of the continuous apparatus. The original apparatus was designed for feeding biomass model compounds soluble in water. The first set of experiments used glucose as a model compound. The organic substrate (glucose) is dissolved in water and an additional water stream is fed using positive displacement piston pumps (Eldex).

Heat is provided by a Mellen three-zone split furnace, 60 cm length, and insulated at top and bottom with 2" thick insulation board (rated to 1150°C) fitted to mesh with the mixing tee, preheat coil, and reactor. Exhaust wrap is also used as insulation around the mixing tee. After exiting the reactor, the reaction is quenched to 25°C in the cooling coil passing through a water bath.

Below the cooling coil is a high-pressure equilibrium phase separator (HEPS) with a volume of 570 ml. The liquid phase is continuously drained via a metering valve, and permanent vapors produced by SCW gasification are metered continuously from the top via a research control valve (Badger Meter Inc.). The components of each phase are detailed below for different sets of experiments. This high pressure separator gives efficient separations with a clean, dry vapor product.

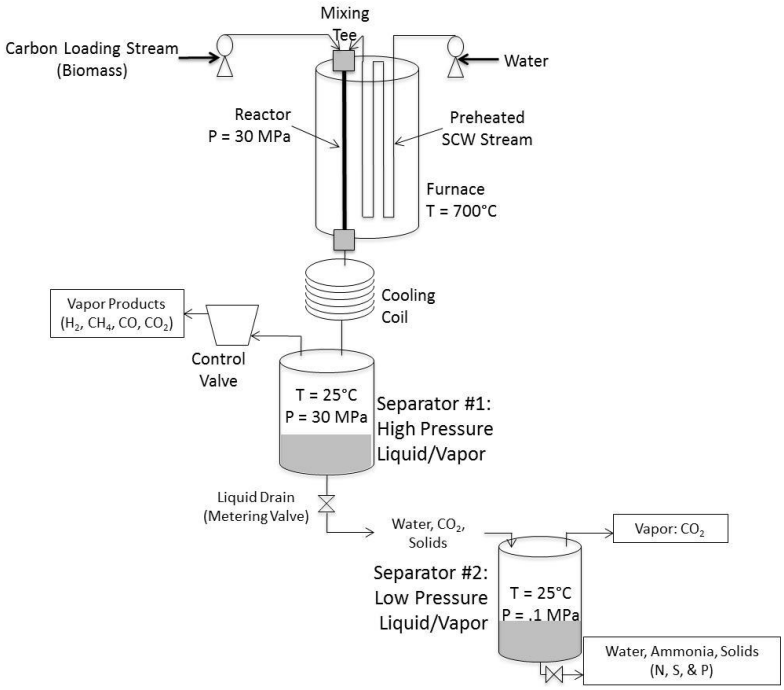

Figure 3.1. Schematic of original continuous thermochemical conversion apparatus built in the CRC.

Two important design features of the SCWG apparatus in Figure 3.1 are different from other approaches (Lee 2002; Hao 2003). First, the water stream passes through a coiled 300 cm length of tubing in the furnace heating the water to supercritical state. This is referred to in this report as the preheat stream. Second is the "Y" shaped mixing tee. The preheated supercritical water from the preheat stream mixes with the carbon loading stream in the mixing tee just prior to entering the main reactor. This mixing method leads to essentially instantaneous heating of the carbon stream which eliminates any undesirable hot water chemistry such as polymerization or charring. For example, when operating at a furnace temperature of 750°C and at a flow rate ratio of preheat stream to carbon loading stream of 1.9:1, the temperature in the mixing tee is 520°, well above the critical temperature of 375°. The temperature continues down the reactor and the final temperature is dependent on the residence time. The sections below have temperature profiles for different experimental conditions. When operating without the preheat stream of water, the carbon stream has a much slower heating rate and the reactor has

a tendency to accumulate char. In some cases, this char buildup causes a clog in the reactor forcing operation to shut down.

3.2 CONTINUOUS REACTOR OPERATION

While different feeds and different feeding mechanisms were used for different experiments, the overall operation of the continuous SCW gasification apparatus was similar. To adapt the apparatus for thermochemical conversions other than gasification required some adaptation and additional steps. The general operation procedure for gasification experiments is detailed below. Refer to Figure 3.1 in section 3.1.

The preheat water stream and carbon feed (biomass and model compounds) were pumped into the reactor. The ratio of water to feed varied from 1:1 to 2:1 on a volume basis at room temperature. The mass flow rates were similar with any difference being accounted for by differences in density between the water and feed. The resultant concentration of feed is the concentration in the mixing tee after the feed stream is mixed with the preheat stream (i.e. the feed stream concentration is diluted by the preheat stream).

The organic stream enters the mixing tee at a temperature slightly above ambient due to heat conducting through the tubing from the furnace. The preheat water stream enters the mixing tee as a supercritical fluid at the temperature of the furnace. The temperature in the mixing tee is a function of furnace temperature and the ratio of flow rates of each stream. With furnace temperatures > 600° and water to feed ratios > 1 the mixture becomes a supercritical fluid virtually instantaneously in the mixing tee. In the combined stream in the mixing tee, both phase changes and sensible heat effects determine the mixture temperature, and the observed values agree closely with values predicted from thermodynamic calculations.

Startup procedure consisted of using a gas booster to pressurize the system with nitrogen gas to >22 MPa (the critical pressure of water). Nitrogen is used because it is inert is

not a product or intermediate of any thermochemical reaction and can be used to help determine when steady state is reached. Once the furnace reached the desired temperature, water was pumped through the preheat stream. After the mixing tee reached 375°C (the critical point of water), the carbon stream was turned on. Inputs of carbon feed and pre-heated water were measured by direct observation of volume dispensed from the reservoirs. Liquid was drained out the bottom of the high-pressure equilibrium phase separator with a metering valve and vapor was released from the separator through the control valve (see Figure 3.1) to maintain constant pressure. Steady state was established when the composition of the vapor stream became constant, (all the nitrogen flushed from the system). Depending on the mass feed rates, reaching steady state to between 15 and 60 minutes.

The density of the reacting fluid is required to determine the average residence time of the reacting fluid in the reactor. From previous experiments in our lab and from literature sources (Kruse 2008; Kersten 2006), it is known that changes in pressure in the range of 22 to 33 MPa do not effect SCW gasification. Therefore, the residence time in the reactor was set by changing pressure in this range. The density of SCW is known from extended steam tables under these conditions and the effect of carbon loading on fluid density is assumed to be small. To justify this assumption, a comparison of the densities of water and a biomass model compound (ethanol) is shown in Table 3.1. Densities are compared over a range of practical operating temperatures. The pressure was maintained at 30 MPa, a representative pressure during operation of the SCW apparatus. Deviations are small enough to justify this approach in calculating residence time. A similar result is obtained when comparing water to other biomass model compounds including glucose and biomass slurries including algae.

	ρ (g/cm^3)		
T (°C)	Water	EtOH	Deviation
600	0.088	0.089	2.1%
700	0.073	0.077	5.6%
800	0.063	0.068	6.4%

Table 3.1. Comparison of densities of water and EtOH as a model compound. P = 30 MPa.

For every experiment at a given set of conditions, two measurements were taken. Once steady state was reached, the liquid metering valve was closed and the pressure of the system was regulated by releasing vapor from the separator via the control valve. A dry test meter was used to measure cumulative vapor production to calculate average vapor flow rate. The difference between the average vapor flow rate when pumping carbon feed and the average vapor flow rate when pumping pure water is due to gasification and fuel gas production. This volumetric net rate, measured at ambient conditions, is directly proportional to molar flow rate and is a key observation. The composition of the vapor produced was determined by gas chromatography (GC, Varian 450with Supelco 30m X 0.53 mm Carboxen 1010 PLOT fused silica capillary analytical column). The analytical column separated CO_2, CO, H_2, CH_4, C_2H_6, O_2 and N_2, which are quantified by thermal conductivity and flame ionization detectors in series.

GC composition data along with vapor flow rates allowed calculation of mole and mass fractions, as well as carbon and hydrogen balances. Five responses are defined as performance metrics for the SCW gasification process. The first is overall gasification efficiency (GE). It is a ratio of the mass rate of vapor coming out to the mass rate of carbon feed pumped in the system at steady state. SCW acts as a solvent, but also acts as a reactant by splitting to contribute hydrogen and oxygen to the reacting fluid. Therefore the overall gasification efficiency is not bound at 100%. However, very few experiments were observed to exceed 100% GE. The second response metric is carbon efficiency (CE), which represents the ratio of carbon in vapor products (CO, CH_4, CO_2, and C_2H_6) to the carbon in the feed reactant. The carbon efficiency is bound at 1 because the only source of carbon is in the feed.

The third and fourth performance metrics, H_2 yield and CH_4 yield, are key metrics to determine the value of the fuel gas produced. H_2 yield is the proportion of hydrogen atoms from the feed that appear in the product mixture as molecular hydrogen. As with GE, it is not bound at 100% because SCW is both a solvent and a reactant; however, H_2 yield has never been observed to exceed 100%. CH_4 yield is the proportion of carbon atoms in the feed that appear as methane in the product mixture and is bound at 100%. H_2 yield and CH_4 yield are not independent, as both are affected by methanation reactions.

The final and perhaps most important metric of interest is gasification rate, in units of concentration per time. Gasification rate is the least studied of all the parameters, but perhaps the most important to the potential commercial viability and profitability of this technology. Table 3.2 shows the formula used to calculate the performance metrics, using glucose as an example. Slight adjustments are made to account for different kinds of feed based on feed composition.

$$GE = \frac{Vapor\ Mass\ Flow\ Rate\ Out}{Glucose\ Mass\ Flow\ Rate\ In} \cdot 100\%$$

$$CE = \frac{Vapor\ Molar\ Flow\ Rate\ \cdot [x_{CO} + x_{CH_4} + x_{CO_2} + 2x_{C_2H_6}]}{6 \cdot Glucose\ Molar\ Flow\ Rate} \cdot 100\%$$

$$H_2\ Yield = \frac{Vapor\ Molar\ Flow\ Rate\ \cdot [2x_{H_2}]}{12 \cdot Glucose\ Molar\ Flow\ Rate} \cdot 100\%$$

$$CH_4\ Yield = \frac{Vapor\ Molar\ Flow\ Rate\ \cdot [x_{CH_4}]}{6 \cdot Glucose\ Molar\ Flow\ Rate} \cdot 100\%$$

$$Rate = \frac{Glucose\ Concentration}{Residence\ Time} \cdot GE$$

Table 3.2. Calculation of Performance Metrics using glucose as an example feed.

3.3 Safety

Working with hot fluids at high pressures presents obvious dangers, so certain safety precautions are needed when operating the SCW continuous reactor. Were an accident to occur, the total amount of hot fluid in the reactor and preheat stream was small, around 50-100 mL depending on the size of reactor in operation. However, at high pressures, even small

amounts of hot fluid can be dangerous. Safety glasses and gloves were always used when operating the reactor. Plexiglas was mounted surrounding the top of the reactor (around the mixing tee) to stop any potential leaks becoming dangerous. During data collection, sheet metal was mounted strategically around the apparatus to shield the operator. During the operation of the original and subsequent apparatuses, several failures occurred causing rapid decompression. However, the safety measures proved effective as there were no injuries during operation. The point of failure was always in the preheat coil when a relatively cold (ambient temperature) water is pumped into a hot tube. This point of failure was eliminated by monitoring the usage of the preheat tubing and replacing after 50 – 100 hours of use.

4. Gasification of glucose as a model compound for biomass: Factorial Experimental Design and Results.

4.1 SUMMARY

The first generation continuous SCW gasification apparatus from Figure 3.1 above is used to investigate glucose gasification in supercritical water at high temperatures and low residence times. A 2^3 full factorial experiment was performed to determine the effects of feed concentration, temperature, and residence time on glucose gasification. The temperature levels (750° and 800°C) were higher than ever used, while the residence times (4 and 6.5 seconds) were shorter than ever used in previous supercritical water gasification studies. The reactor proved capable of attaining higher gasification rates than previously shown with high efficiencies and yields. In addition, the glucose gasification reaction was modeled by estimating activation energy and reaction order of glucose gasification in supercritical water. Based on previous experiments in our laboratory and from examination of Table 2.2 in section 2.2, several hypotheses were developed as the focus of this report:

H_1: In SCWG, higher concentrations, higher temperatures, and faster residence times lead to highest gasification rates, but not necessarily the highest efficiencies or yields.

H_2: Heating rate is an important parameter in SCW gasification. Fast heating eliminates hot water chemistry during heat up and produces higher yields and efficiencies.

H_3: SCWG leads to clean separations.

H_4: High temperature gasification has no need for catalysts, which are undesirable economically and operationally.

Operating procedures for the continuous gasification apparatus are in section 3 above. Two different reactors were used in this set of experiments. The large (1.43 cm OD, 0.64 cm ID)

and small (0.95 cm OD, 0.52 cm ID) reactors were used to operate at long and short residence times, respectively.

4.2 STATISTICAL DESIGN OF EXPERIMENTS

A 2^3 full factorial experimental design was used to evaluate the effect of three variables on the process performance metrics defined above. The variables were: feed concentration (C), temperature (T), and average residence time (τ). The design requires each variable be assigned two factor levels, designated as plus and minus (Box 2005). These factors and their levels are shown in Table 4.1. The temperature levels were higher and the residence times shorter than almost all previous studies. Concentration levels were in the range of practical interest and catalysts were not included. These levels were selected in accordance with hypotheses stated above pertaining to the most practical and promising conditions under which to operate.

Effect	Abbreviation	Minus Level (-)	Plus Level (+)
Glucose Concentration	C	10%	15%
Furnace Temperature	T	750˚C	800˚C
Residence Time	τ	4 sec	6.5 sec

Table 4.1. Variable low and high levels used in factorial experiment.

Table 4.2 shows experimental design in standard order, not necessarily the order in which the experiments were performed). Because this is a full factorial experiment, every combination of plus and minus levels of C, T, and τ are included in the 8 runs, allowing for direct comparisons. In addition to the factorial runs presented in this report, experiments with the same apparatus were done using a reactor equipped with thermocouple points located 20 cm and 40 cm inside the 60 cm reactor to measure the temperature of the flowing fluid directly. At the ambient operational flow rate of 10.5 ml/min, average fluid temperature was dependent of furnace temperature and not feed concentration or residence time. At a furnace temperature of 750°C, average fluid temperature was 740°C; at a furnace temperature of 800°C, average fluid

temperature was 790°C. These fluid temperatures were used to calculate density and residence time.

Run	C	T	τ
1	-	-	-
2	+	-	-
3	-	+	-
4	+	+	-
5	-	-	+
6	+	-	+
7	-	+	+
8	+	+	+

Table 4.2. Factorial Experiment Setup in standard order.

4.3 RESULTS AND DISCUSSION

Table 4.3 presents the raw data from the eight-run, full factorial experiment along with the five calculated responses defined above. Several runs had over 100% CE due to experimental error; since CE is bound at 1, these runs were reported at 100% in Table 4.3. Eight experiments allow estimation of 8 parameters; the three main effects (C, T and τ), their 3 possible two-way interactions and their three-way interaction, as well as the overall average.

	Gas Phase Mole Fractions					Gasification Efficiencies and Yield				Gasification
Run	H_2	CO	CH_4	CO_2	C_2H_6	GE	CE	H_2 Yield	CH_4 Yield	Rate (g/L-s)
1	0.40	0.22	0.18	0.17	0.03	73.0%	75.7%	47.6%	43.1%	18.6
2	0.26	0.48	0.13	0.09	0.04	47.4%	52.7%	17.1%	17.7%	18.4
3	0.36	0.33	0.15	0.11	0.05	103.3%	100%*	59.5%	50.8%	26.2
4	0.23	0.41	0.17	0.14	0.05	93.5%	100%*	28.7%	42.7%	36.0
5	0.30	0.42	0.14	0.10	0.05	102.2%	100%*	44.8%	40.8%	15.8
6	0.30	0.31	0.12	0.25	0.02	56.0%	52.9%	22.0%	17.4%	13.2
7	0.34	0.01	0.26	0.32	0.06	117.5%	100%*	57.0%	86.4%	18.3
8	0.28	0.32	0.16	0.17	0.08	79.1%	87.1%	30.5%	34.8%	18.7

Table 4.3. Raw Data from Factorial Experiment.
*CE calculations were over 1 due to small experimental error, but reported here as 100% because unlike GE, CE is bound at 1.

Normal probability analyses were used to determine which variables and their interactions had a significant effect on the responses, and which were on the level of the noise.

Figure 4.1 shows the normal probability plot for the gasification rate response. In the figure, T and τ are labeled because they appear to be outliers and are deemed as having a significant effect on gasification rate. The same process is done for the other 4 responses.

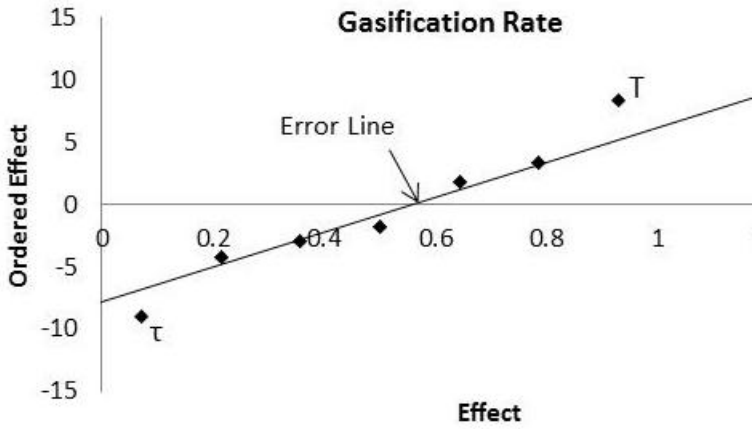

Figure 4.1. Normal probability plot for the gasification rate parameter. It is clear from normal probability analysis that T and τ deviate beyond the level of the noise and are thus significant parameters.

Next, as prescribed for factorial experiments without replication, the standard error is estimated by calculating a pooled variance using the effects and interactions deemed not significant (Box 2005). The standard error was also evaluated using Lenth's analyses and comparable values were obtained. These are the values included as standard error lines in the Lenth plots in Figure 4.2. Any effect that is less than or on the order of the standard error is considered unimportant, within the limited range of the factor-levels, while any effect much larger than the standard error is significant. Figure 4.2 has five parts (a through e) that correspond to each response defined above. It illustrates the sign and magnitude of each effect and interaction as departures from the overall average, as well standard error lines for judgments of significance.

Consider the first column in Figure 4.2-A, which shows the effect of concentration (C) on gasification efficiency (GE). The column indicates that the average gasification efficiency of the four runs conducted at the minus level (10 wt%) was 30% higher (85% minus 55% GE) than the

average gasification efficiency of the four runs conducted at the plus level (15 wt%). This variable had a similar negative effect for carbon efficiency (CE), as shown by the first column in Figure 4.2-B. Both H_2 yield and CH_4 yield also decrease with increasing concentration (Figures 4.2-C and 4.2-D), however, the gasification rate did not change outside the level of the noise (Figure 4.2-E). In this manner, the magnitude and sign of each main effect and interaction can be considered independently for each of the five responses.

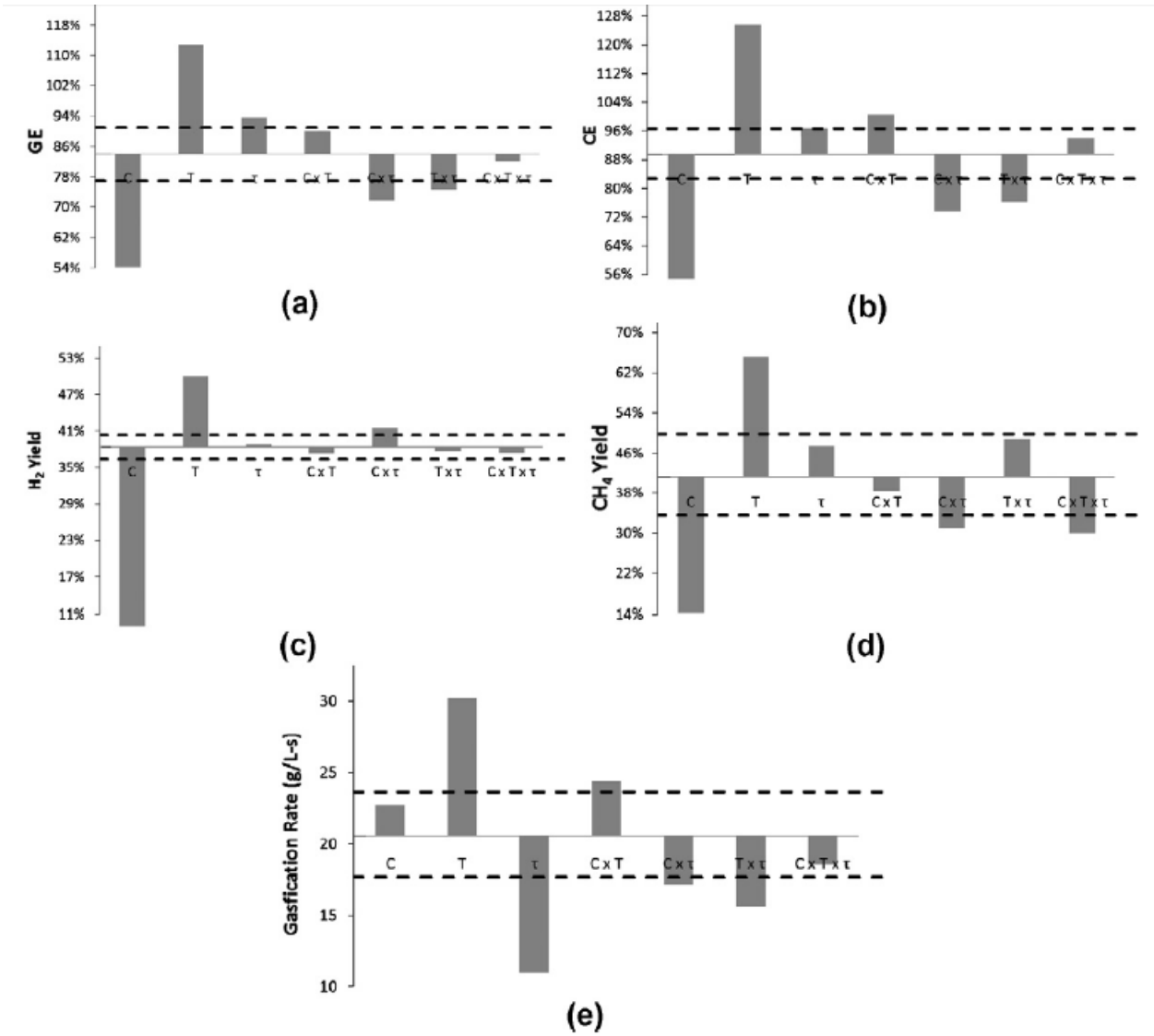

Figure 4.2. Lenth Plots of Main Effects and Standard Error of all five response metrics.

4.4 INTERPRETATION OF RESULTS

As shown in Figure 4.2, going from 750° to 800° increased all five metrics significantly. Although final temperature determines reaction rate, it is also hypothesized that heating rate is an important parameter in SCW gasification. The higher furnace temperature allowed for higher mixing tee temperatures and thus higher heating rates of the feed stream, as well as a higher final temperature.

Feed concentration is a significant variable for efficiencies and yields, but not rate. Increasing the feed concentration from 10 wt% to 15 wt% decreased gasification and carbon efficiencies, H_2 and CH_4 yield, but had no significant effect on rate. While it was predicted that higher concentrations would lead to lower efficiencies and yields, these results contradict the hypothesis that higher concentrations lead to higher gasification rates. At higher concentrations it is possible that polymerization reactions resulting in formation of recalcitrant species reduce the number of glucose molecules available for decomposition (gasification). In batch reactor studies, it was observed that glucose, which is soluble in liquid water and in SCW, gasifies less efficiently than a broad spectrum of biomass (Venkitasamy 2011). Most biomass is insoluble in liquid water but becomes more soluble in SCW. "Hot water chemistry" may be important for liquid water-soluble model compounds despite the rapid heating rate featured in this apparatus.

Increasing residence time from 4 to 6.5 seconds decreased gasification rate by an estimated 8 g/L-s. Our second hypothesis was that faster residence times would lead to increased gasification rates, but not necessarily higher efficiencies and yields. It was confirmed that faster residence times are advantageous to rate, yet this increase in rate did not come at the expense of the other metrics as neither efficiency or yield was significantly affected by changing the residence time in this range. As mentioned, residence times of 4 and 6.5 seconds were much shorter than ever previously reported.

Two interactions were found to be important: C x τ had an effect on both GE and CE, and T x τ had an effect on CE. The decrease in GE and CE due to increasing concentration from 10% to 15% is greater at slower residence times than at faster residence times. Additionally, the increase in CE due to increasing temperature from 750 to 800° is greater at slower residence times than at faster residence times. The C x τ and T x τ interactions only effected GE and CE and not the other performance metrics.

4.4 COMPARISON TO OTHER GLUCOSE GASIFICATION STUDIES

Table 2.2 in section 2.2 summarizes previous reports of glucose gasification in SCW from the literature. Figure 4.3 displays gasification rate and efficiency data from reports done with continuous reactors (not batch reactors) along with data from this report. Rate and efficiency data were recalculated from each reference using the same procedure as shown in Table 3.2 in section 3.2. All the studies presented show efficiencies close to or greater than 100%. The gasification rate showed much greater disparity between the different reports. The data reported here produced a maximum glucose gasification rate of 36 g/L-s. Relative to the highest rate previously reported (Xu 1996), a nearly six-fold increase in rate is achieved while maintaining comparable efficiency. This rate was achieved, as expected, during the factorial run that combined high concentration (15%), high temperature (800°C) and short residence time (4 s). This highlights the utility of the preheat coil and mixing tee approach, which achieves a very high heating rate.

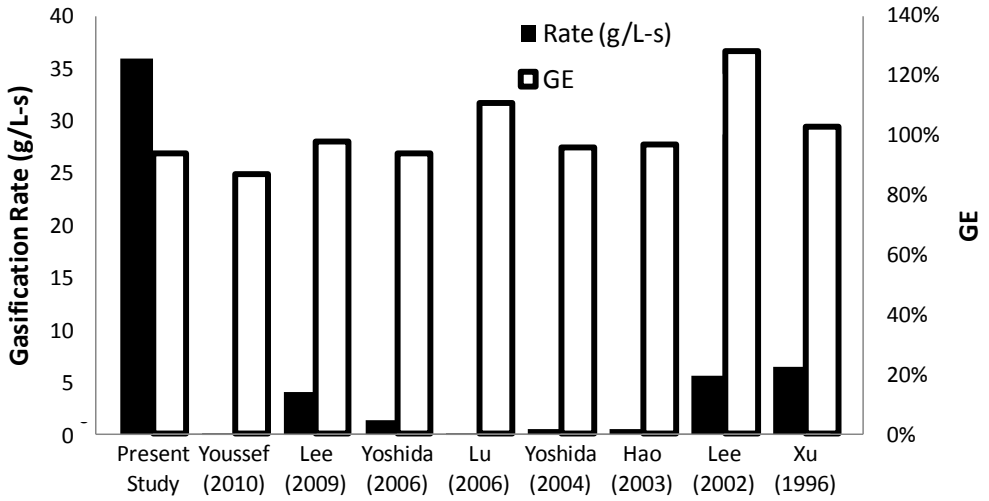

Figure 4.3. Gasification rates and gasification efficiency of several continuous SCW glucose gasification studies.

4.5 QUANTIFYING VAPOR LOST IN LIQUID STREAM

The high pressure liquid/vapor phase separator allowed for clean, efficient separations. Liquid was drained out the bottom of the separator with a metering valve and vapor was released with a control valve (see Figure 3.1 in section 3.1). However, at pressures of over 24 MPa, CO_2, and possibly other vapors, are soluble in water. To quantify vapor solubility, vapor/liquid equilibrium analysis was done on the separator. Vapor mole fractions were known from experimental results and used to find liquid mole fractions using Henry's Law. Henry's Law is applicable for dilute solutions and when there is no saturation pressure, i.e. the temperature in the separator is greater than the critical temperature of the species. The critical temperatures of H_2 (-240°), CO (-140°), and CH_4 (-82°) are well below the operating temperature while the critical temperatures of CO_2 (31°) and C_2H_6 (32°) are slightly higher than operating temperature of 25°, but the concentration is dilute enough that Henry's Law should apply to all species.

It was found that solubility of H_2, CO, CH_4, and C_2H_6 are negligible in water at these conditions (T ≈ 25°, P ≈ 25 MPa). CO_2 had a liquid phase solubility mole fraction of about 3%.

Any variation in the liquid phase solubility of CO_2 was due to variation in the vapor phase product. Experimental results from outside researchers (Sabirzyanov 2003) as well as from our lab confirm this calculation. Liquid solubility of CO_2 actually presents great potential for increasing the degree of separation of the vapor product. Additional phase separators give the apparatus the ability to remove CO_2 from the gasification vapor product stream giving a relatively pure stream of H_2 and CH_4, a very valuable mixture. This additional carbon capture separation step is explored in section 6.

4.6 CALCULATION OF ACTIVATION ENERGY.

Gasification of organic compounds is composed of several reactions occurring simultaneously. In the SCW reactor, these reactions include but are not limited to methanation, water-gas shift, and water splitting. The net effect of all of these individual reactions can be described by the following overall glucose gasification reaction, which includes all the major vapor products:

$$C_6H_{12}O_6 + aH_2O \rightarrow bCO_2 + cCO + dCH_4 + eH_2 + fC_2H_6$$

The temperature dependence of the overall reaction was modeled by the Arrhenius equation, given below.

$$\frac{d[C]}{dt} = -kC^n \quad \text{where} \quad k = Aexp(\frac{-E_a}{RT})$$

Here, C is the feed concentration, k is the specific reaction rate, E_a is the activation energy, A is the pre-exponential factor, n is the reaction order, and d[C]/dt is the gasification rate.

Previous reports of glucose gasification have studied the reaction by assuming a first order reaction, i.e. n = 1 (Bobleter and Pape 1968, Lee 2002, Matsumura 2005). However, for the conditions in this study, feed concentrations in the range of 10-15% were determined to have no effect on gasification rate (although increasing C did show a decrease in efficiency and yield; see Interpretation of Results section). This means that the gasification reaction is zero

order, i.e. n = 0 under the conditions studied. For n = 0, the parameters of the Arrhenius equation were estimated from double reciprocal plots. The value for E_a was 96 kJ/mol and the value for A was 1.2 X 10^6 g/L-s. The same procedure was carried out assuming first order kinetics (n = 1). The value for E_a was estimated to be 70 kJ/mol, and A was estimated to be 1200 s^{-1}.

4.7 FEASIBILITY AND FOOTPRINT OF SCW GASIFICATION TECHNOLOGY

Several companies are in the process of making gasification a commercial process. For example, Enerkem has built a plant in Edmonton, which began commercial operation in 2011. It aims to process 100,000 dry tons of municipal solid waste per year (Enerkem 2010). In an effort to understand the viability of SCW gasification on a commercial scale, the volume of a SCW gasification reactor required to treat this volume was determined. Required assumptions include full time operation, gasification efficiency of 90%, feed density of 1 kg/L, and a dry feed concentration of 20 wt% on a wet basis. The continuous feed gasification process is modeled with a tubular plug flow reactor (Fogler 2004), as follows.

$$V = \int_{F_{S1}}^{F_{S0}} \frac{dF_S}{-r_S} = \int_{F_{s1}}^{F_{s0}} \frac{dF_s}{-Aexp(\frac{-E_a}{RT})C^n} \qquad \text{where} \qquad C = \frac{F_S}{Q}$$

Here, V is the reactor volume, F_{s0} and F_{s1} are the molar flow rates of the solid feed in the inlet and outlet of the reactor, r_s is the gasification rate as defined by the parameters of the Arrhenius equation, which are estimated experimentally. Q is the volumetric flow rate. F_{s0} and F_{s1} are determined by the feed concentration, GE and throughput.

Required reactor volume is based on a throughput of 100,000 ton/year and the other assumptions listed above is computed as a function of temperature for both n = 0 and n = 1. The results of this computation are illustrated in Figure 4.4. Assuming n = 0, the reactor volume at 800° is 100L, a compact industrial reactor. If n = 1, the reactor volume is much smaller. It is

possible that the kinetics of the gasification reaction is between n = 0 and n = 1. This figure illustrates the small footprint of the SCW gasification technology and supports our hypothesis that high temperatures are important for economic viability. Operation at high temperatures allows sufficiently high rates without the use of catalysts, which are undesirable operationally.

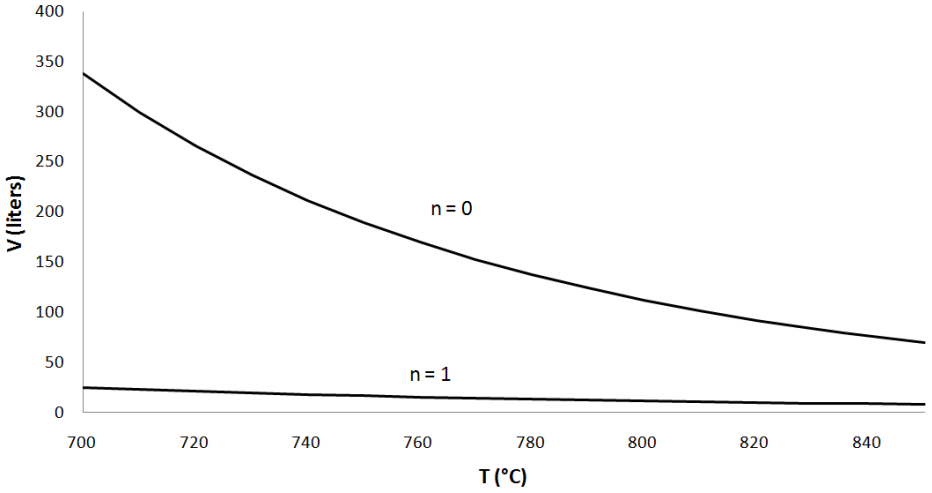

Figure 4.4. Up-scaled model of temperature vs. reactor volume of the gasification process to show feasibility of commercialization. Assumptions include full time operation, gasification efficiency of 90%, feed density of 1 kg/L, dry feed concentration of 20 wt% on a wet basis, and a total throughput of 100,000 dry tons per year.

4.8 CONCLUSIONS

The SCWG continuous apparatus used in these experiments featured a pre-heat coil and mixing tee that provide very high heat up rate. It proved capable of gasifying glucose nearly six times faster than previously reported. Increasing reaction temperature from 750° to 800°C showed large increases in efficiencies (+29% for GE), yields, and gasification rate (+8 g/L-s). Increasing feed concentration from 10% to 15% showed large decreases in efficiency (-30% for GE), and yields, but showed no significant change in rate. Decreasing residence time from 6.5 to 4 seconds in the reactor showed no change in yield despite showing a decrease in efficiency (-9% for GE), but did increase gasification rate by an estimated 8 g/L-s.

5. Gasification of Alcohols as Model Compounds: Overcoming Axial Gradients During Thermochemical Conversion.

5.1 SUMMARY

Supercritical water gasification of ethanol and butanol as biomass model compounds in the continuous supercritical water gasification reactor was explored over a range of residence times from 0.7 to 34 s. Residence time was decreased until turbulence was achieved ($\tau \leq 1.2$ s). As fluid transitioned from laminar to turbulent flow, gasification rate was maximized while gasification efficiency was reduced. Gasification rates up to 107 g/L-s were observed; this is nearly an order of magnitude higher than previously reported. Arrhenius parameters were estimated to model the intrinsic kinetics of gasification of model compounds in supercritical water under plug flow and without any transport limitations in the radial direction (i.e. turbulence); this technique has never before been applied to supercritical water gasification. The effect of feed composition, enthalpy of gasification, and residence time on product composition was also explored.

5.2 EXPERIMENTAL METHODS

The continuous SCWG apparatus described above (see Figure 3.1 in section 3.1) was used for all experiments. The positive displacement pumps were replaced with syringe pumps (ISCO 260D). As before, there was one pump for the preheat stream (pure water) and one pump for the carbon loading stream. Two differently sized reactors were used. The large (1.4 cm OD, 0.6 cm ID) and small (1.0 cm OD, 0.5 cm ID) reactors were used to operate at relatively longer and shorter residence times, respectively.

1-Butanol (BuOH) and ethanol (EtOH) were used as the carbon source in the carbon loading stream. Both alcohols gasify well, are non-toxic, and easy to pump using syringe pumps. The oxygen composition of BuOH is 22 wt%; EtOH is 35 wt%. It is known that the amount of

oxygen in the carbon stream during gasification effects the composition of the vapor product and higher oxygen concentration in the carbon stream will increase CO_2 and decrease the value of the product (Venkitasamy 2011).

Both EtOH and BuOH have an average oxidation state of 2 for their carbon atoms. Therefore, they have similar (mass-based) values for standard change in enthalpy of combustion (kJ/g), which will be negative reflecting the exothermic nature of combustion (the same value reported as a positive number is the "Low Heating Value"). A report from our lab (Venkitasamy 2011) reports they will also have similar values for the change of enthalpy of gasification, however these values will be positive reflecting the endothermic nature of the SCWG overall reaction.

Operational procedures including startup processes and data collection are the same as with the previous set of experiments with glucose. Vapor flow rates at steady state were between 0.5 and 12 L/min at ambient conditions. Vapor samples were collected downstream of the pneumatic valve. GC analysis showed pure vapor samples with no air. The volume of the reactors is relatively low (9 – 19 ml) and a steady state product mixture is achieved quickly. However, the volume of the HEPS is larger (570 ml). Reaching steady state from startup took between 20 and 40 minutes depending on the flow rate, but the system was run for up to 60 minutes before taking a vapor sample.

One of the most important variables is residence time (see Experimental Design section). The density of the reacting fluid is required to determine the average residence time of the reacting fluid in the reactor. The residence time is determined by the reacting fluid density (a function of temperature and pressure), the volume of the reactor and the mass flow rate in each stream. Fluid temperature is known from reactor temperature profiles as described below and in Figure 5.1. From previous experiments in our lab and from literature sources

(Kruse 2008, Kersten 2006), it is known that changes in pressure in the range of 22 MPa to 33 MPa do not have any effect on SCW gasification, however the pressure was maintained in all experiments at 27.6 MPa (4000 psi). The density of SCW is known from extended steam table values of specific volume at high temperature and pressure, with an average temperature used from the fluid temperature profile of each run. From the average fluid density (from the average fluid temperature) and reactor volume, the mass flow of both the preheat stream and carbon loading stream was adjusted to determine residence times. The ratio of flow rates of these two streams was maintained to maintain constant mixing tee temperatures between different runs. The effect of the carbon loading stream on fluid density is assumed to be small. This assumption was validated by using the Peng Robinson equation of state to estimate the densities of pure EtOH and pure BuOH at the conditions of interest in this investigation. The alcohols were SCFs and had similar densities to SCW at the temperatures and pressures of interest. Table 5.1 below shows the results of the comparison of water and EtOH. A relatively high water to carbon flow rate ratio, instantaneous mixing and high gasification efficiency further support this assumption.

	ρ (g/cm^3)		
T (°C)	Water	EtOH	Deviation
600	0.088	0.089	2.1%
700	0.073	0.077	5.6%
800	0.063	0.068	6.4%

Table 5.1. Comparison of densities of water and EtOH as a model compound. P = 30 MPa.

5.3 EXPERIMENTAL DESIGN

In section 3.2 there were five responses defined as performance metrics for the SCW gasification process. In this set of experiments the focus was on GE and gasification rate. The rate, as defined here, only includes the amount of feed fully converted into vapor product and does not include any liquid intermediates. There are many reports that address intermediates in supercritical water gasification of biomass and model compounds (Savage 1999, Yoshida

2001). Gasification rate has not been optimized in the literature, but will determine commercial viability of SCWG technology.

Table 3.2 in section 3.2 defines the metrics for glucose; GE and rate are also defined below for EtOH. Here, $\dot{m}$ represents mass flow (g/min), C is mixing tee concentration (g/L), τ is residence time (s). EtOH is used as an example for both carbon species. Parameters for BuOH are found in the same way.

$$\%GE = \frac{\dot{m}_{H_2}+\dot{m}_{CO}+\dot{m}_{CO_2}+\dot{m}_{CH_4}+\dot{m}_{C_2H_6}}{\dot{m}_{EtOH}} \cdot 100\% \qquad Rate = \frac{C}{\tau} \cdot \%GE$$

Ten experiments were run for each carbon species, each run being the average of two or three replications, which established repeatability and provided a basis for estimation of uncertainty. The furnace temperature was maintained at 750°C, the mixing tee carbon stream concentration was maintained at 0.28 g/mL for BuOH and 0.27 g/mL for EtOH; the difference is accounted for by density differences between the two species. The residence time was varied from 0.7 to 34 seconds. A residence time of 30 seconds is relatively fast compared to most SCW gasification studies. A residence time of 0.7 seconds was chosen to ensure turbulent, plug flow conditions were achieved. This range of residence times is appropriate to produce high rates while maintaining moderate to high efficiencies. A temperature of 750°C is a relatively high gasification temperature compared to other studies, enabling complete gasification without use of catalysts (Hendry 2011). The conditions of this first set of experiments are summarized in Table 5.2, along with the raw data (see section 5.5 for analysis of results). A mass balance was performed after data collection to ensure data was sensible. The ratio of water to carbon feed, and thus, the mixing tee concentration, is maintained constant in each run for each species. The water stream is the flow through the preheat coil. The standard run number is used for bookkeeping and not the order the experiments were performed.

Run No.	$T_{furnace}$ (°C)	Reactor	Water Stream (ml/min)	EtOH Stream (ml/min)	EtOH Flow (g/min)	τ (s)	EtOH %GE	EtOH Rate (g/L-s)
E1	750	Small	37	19	15	**0.67**	**19.0%**	**101.9**
E2	750	Small	27	14.3	11	**1.2**	**39.8%**	**107.6**
E3	750	Small	14	7.14	5.6	**2.4**	**67.1%**	**94.5**
E4	750	Small	9.4	5.0	3.9	**3.7**	**76.4%**	**68.9**
E5	750	Small	7.7	4.1	3.2	**4.8**	**82.4%**	**55.9**
E6	750	Large	7.8	4.1	2.5	**8.4**	**86.1%**	**39.1**
E7	750	Large	5.3	2.8	1.5	**12**	**93.7%**	**25.4**
E8	750	Large	4.3	2.3	1.2	**15**	**95.6%**	**20.9**
E9	750	Large	2.7	1.4	0.74	**23**	**96.1%**	**13.1**
E10	750	Large	1.8	0.94	0.49	**34**	**95.3%**	**8.7**

Run No.	$T_{furnace}$ (°C)	Reactor	Water Stream (ml/min)	BuOH Stream (ml/min)	BuOH Flow (g/min)	τ (s)	BuOH %GE	BuOH Rate (g/L-s)
B1	750	Small	37	19	15	**0.67**	**16.5%**	**91.4**
B2	750	Small	27	14.3	12	**1.2**	**34.4%**	**96.4**
B3	750	Small	14	7.14	5.8	**2.4**	**49.5%**	**72.2**
B4	750	Small	9.4	5.0	4.0	**3.7**	**64.7%**	**60.4**
B5	750	Small	7.7	4.1	3.3	**4.8**	**78.2%**	**54.8**
B6	750	Large	7.8	4.1	3.3	**8.4**	**78.9%**	**36.8**
B7	750	Large	5.3	2.8	2.3	**12**	**82.6%**	**23.0**
B8	750	Large	4.3	2.3	1.8	**15**	**82.8%**	**18.6**
B9	750	Large	2.7	1.4	1.1	**23**	**85.9%**	**12.0**
B10	750	Large	1.8	0.94	0.76	**34**	**84.2%**	**7.9**

Table 5.2. Summary of experimental conditions and raw data.

After analyzing the results of the set of experiments in Table 5.2, a second set of experiments was performed, all of which were at turbulent conditions (see Section 5.5). The conditions of these experiments are summarized in Table 5.3 along with the raw data. Runs 11-16 were done with pure alcohol while runs 17-19 were run with each alcohol diluted with water in the carbon stream so that reaction order, n, could be determined as described in section 5.7. Note the run number was for bookkeeping and not the order in which the experiments were performed and each data point is the average of replicate runs.

5.4 FLUID TEMPERATURE PROFILE

In order to complete the thermodynamic analysis on the results given in section 5.7, the fluid temperature is required. Using thin thermocouples plumbed into the system, direct temperature measurements of the fluid were taken at five points in the reactor: the mixing tee,

the reactor exit, and three evenly spaced points in between. These measurements, which allow estimation of activation energy in section 5.7, were taken at the conditions in Table 5.2 and Table 5.3. The small change in volume due to addition of the thermocouples was accounted for in residence time calculations and shown through replicate runs not to effect response parameters (%GE, gasification rate). These direct measurements give a reliable temperature profile in the reactor and are necessary for estimation of activation energy in section 5.7.

Run No.	$T_{furnace}$ (°C)	Water Stream (ml/min)	EtOH Stream (ml/min)	EtOH Flow (g/min)	C_{EtOH} (g/l)	***EtOH***	
						GE	***Rate (g/L-s)***
E11	720	20.9	8.4	6.6	225	18% ± 1.3%	34.1 ± 1.4
E12	720	19.4	10.3	8.1	273	17% ± 1.5%	39.3 ± 3.4
E13	750	20.1	8.1	6.4	225	40% ± 1.4%	76.3 ± 2.7
E14	750	18.7	9.9	7.8	273	39% ± 1.2%	89.5 ± 2.7
E15	780	19.4	7.8	6.1	225	45% ± 2.0%	85.3 ± 3.8
E16	780	18.0	9.5	7.5	273	43% ± 1.5%	98.5 ± 3.5
E17	720	19.4	10.3 (82%EtOH)	6.6	225	18% ± 0.8%	33.2 ± 1.6
E18	750	18.7	9.9 (82%EtOH)	6.4	225	41% ± 1.3%	77.3 ± 2.4
E19	780	18.0	9.5 (82%EtOH)	6.2	225	45% ± 1.5%	84.3 ± 2.8

Run No.	$T_{furnace}$ (°C)	Water Stream (ml/min)	BuOH Stream (ml/min)	BuOH Flow (g/min)	C_{BuOH} (g/l)	***BuOH***	
						GE	***Rate (g/L-s)***
B11	720	20.8	8.3	6.7	231	18% ± 0.4%	34.2 ± 0.5
B12	720	19.3	10.2	8.3	280	16% ± 0.8%	36.7 ± 1.9
B13	750	20.0	8.0	6.5	231	36% ± 1.6%	70.8 ± 3.1
B14	750	19.3	10.2	8.3	280	33% ± 1.8%	77.2 ± 4.3
B15	780	19.3	7.7	6.3	231	41% ± 1.2%	79.8 ± 2.3
B16	780	17.9	9.5	7.7	280	37% ± 1.8%	88.0 ± 4.3
B17	720	19.3	10.2 (85%BuOH)	7.0	231	16% ± 1.9%	31.8 ± 3.7
B18	750	18.5	9.8 (85%BuOH)	6.8	231	35% ± 1.0%	67.3 ± 1.9
B19	780	17.9	9.5 (85%BuOH)	6.5	231	39% ± 1.7%	75.5 ± 3.2

Table 5.3. Raw data of gasification experiments with τ = 1.2 s.

Figure 5.1 displays the temperature profiles down the length of the reactor (z) for a representative number of residence times for the experiments in Table 5.2. Temperature profiles were independent of feed, thus both EtOH and BuOH showed the same profile for each respective residence time. It should be noted that all 10 runs for both EtOH and BuOH had unique temperature profiles; Figure 5.1 only shows four of these profiles. Runs done at shorter residence times meant the fluid had less time in the hot reactor, and thus a lower temperature

at each respective vertical position. Thus, fluid temperature and residence are not independent of one another. A polynomial function was fit to the five direct temperature measurements, and the data points are shown for the shortest residence time. For each curve, the correlation was $R^2 > .98$. Due to the vertical orientation of the furnace and less than perfect insulation, a "chimney effect" was seen at the exit of the reactor and was more pronounced at longer residence times.

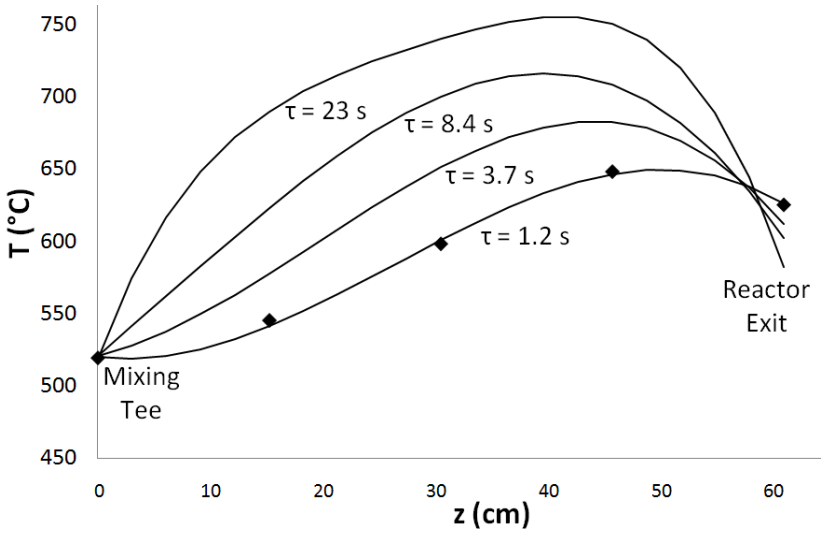

Figure 5.1. Temperature profile for a representative number of runs from Table 5.2.

5.5 PIPE FLOW AND REYNOLDS NUMBER IN RELATION TO %GE AND GASIFICATION RATE.

Turbulent flow ensures axial mixing, eliminating axial temperature and concentration gradients. The transition from laminar to turbulent flow was examined by calculating the Reynolds number (Re) for each experiment in Table 5.2. In pipe flow, Re = VD/v where V is average fluid velocity (m/s), D is the inner diameter of the pipe (m), and v is the kinematic viscosity (m^2/s). The kinematic viscosity is the dynamic viscosity, μ (kg/m-s), divided by density, ρ (kg/m^3) ($v = \mu/\rho$). Values of μ for SCW were taken from data by Walton (1960) and values of ρ for SCW where found from extended steam table enthalpy data. The reacting fluid was assumed to be all SCW. This assumption was validated as described in section 5.2 with the Peng Robinson equation of state and supported by a relatively high water to carbon flow rate ratio,

instantaneous mixing and high GE. For pipe flow, a Reynolds number above about 4000 indicates turbulent flow for all any fluid mixture including a supercritical fluid mixture such as the one in the reactor. The use of Re is to indicate the onset of turbulence. With no conversion, the assumption that alcohols have similar properties to water is true by the Peng-Robinson equation of state. As conversion occurs, velocity increases proportionally to the decrease in density so that pressure is maintained and viscosity is the only variable that affects Re. Conversion of feed to vapor will decrease viscosity (increase Re) down the length of the reactor. However, increasing Re down the length of the reactor is noteworthy, but not necessary to estimate the onset of turbulence so that any plug flow is observed and transport limitations in the radial direction are overcome. Thus, the point at which we estimate onset of turbulence in Figure 5.2 is conservative and the basis for the rest of the experiments in Table 5.3.

Figure 5.2 shows the gasification rate and %GE against Re with 95% confidence intervals, as well as representative residence times. The results presented here are the average of duplicate runs for each experiment ($2 \leq n \leq 3$). EtOH achieved slightly better gasification than BuOH at each residence time (and Reynolds number) as well as a higher maximum efficiency. As mentioned, the average oxidation state of the carbon atoms in EtOH is more negative. This property does not correlate with %GE (Venkitasamy 2011), but does affect the vapor product quality (see section 5.8).

Examination of Table 5.2 reveals that the maximum attainable gasification efficiencies (96% for EtOH and 86% for BuOH) are essentially achieved in less than 12 s residence time. Residence times above 12 s did not significantly improve gasification. Residence times less than 5 s observe a steep drop in efficiency, however such short residence times are needed to eliminate axial gradients in temperature and concentration and achieve maximum rate. Both temperature and residence time are known to effect %GE. The steep drop in %GE here is

accounted for by the decreasing residence time as well as the drop in temperature associated with such a drop in τ (see temperature profiles in Figure 5.1). Several reports have estimated the effects on %GE with changing temperature and residence time (Kruse 2008; Hendry 2011; Peterson 2008). The results in Figure 5.2 give insight into future SCWG reactor design. An ideal reactor will maintain sufficiently high linear velocity to maintain high Re (maximum rate), and will have a large reactor length to produce sufficiently long residence time (maximum %GE).

As hypothesized, the gasification reactions achieved maximum rate in the turbulent flow region (Re > 4000). Further increasing Re did not enhance axial mixing or increase rate. At residence times below 2 s, conversion is low, but rate is maximized. These conditions are necessary for the analysis of intrinsic rate data described in section 5.6 (Fogler 2004).

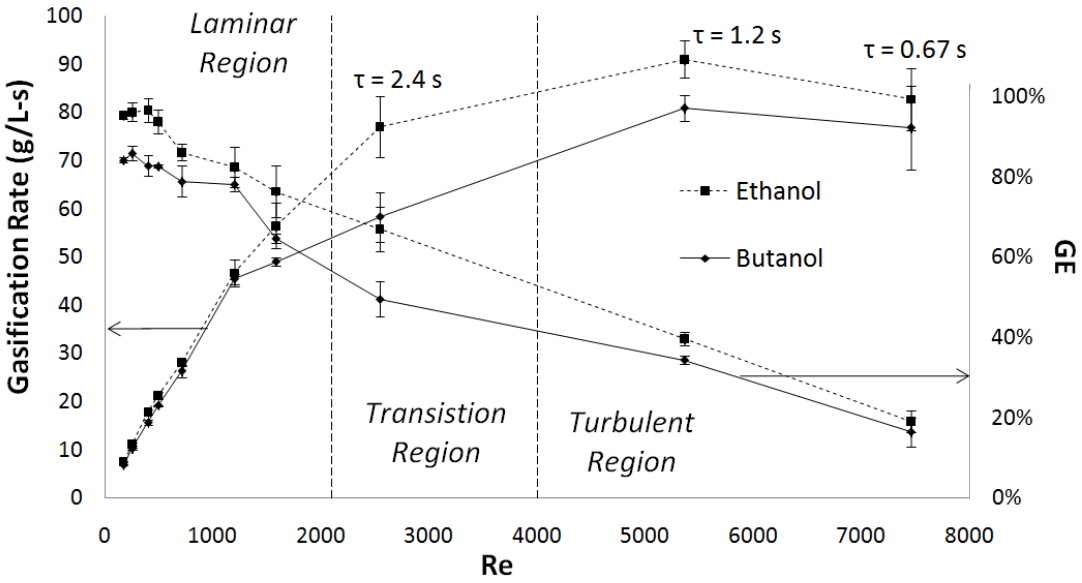

Figure 5.2. Relationship of Reynolds number against gasification rate and GE with 95% confidence intervals.

5.6 INTRINSIC RATE OF SCW GASIFICATION DURING TURBULENT OPERATION.

Gasification of organic compounds in SCW is thermal decomposition in the absence of oxygen. Several additional reactions also occur. In the SCW reactor, these reactions include but are not limited to methanation, water–gas shift, and water splitting. The net effect of all of these is quantified by the overall gasification reaction efficiency and rate. As mentioned above,

turbulent, plug flow operation was achieved in the SCW reactor when $\tau \leq 1.2$ s. Table 5.3 details the additional experiments that were performed at high Re/low τ in the temperature range around 750°. The gasification rate is modeled by the power law: $\frac{d[C]}{dt} = -kC^n$ where k is given by the Arrhenius equation: $k = Aexp(\frac{-E_a}{RT})$. The Arrhenius equation is used to account for temperature dependence on reaction rate (Fogler 2004). Here, C (g/L) is the feed concentration, k ($(g/L)^{1-n}/s$) is the specific reaction rate, E_a is the activation energy (kJ/mol), A ($(g/L)^{1-n}/s$) is the pre-exponential factor, n is the reaction order, and d[C]/dt (g/L-s) is the gasification rate.

For these additional experiments, residence times were held at 1.2 s to ensure turbulent flow and allow observation of intrinsic rate. Furnace temperature was set at 720°, 750°, and 780°C which was determined to be a small enough temperature range for good accuracy but large enough to see significant differences in gasification between temperature settings. Mixing tee concentrations used were 225 and 273 g/L for EtOH and 231 and 280 g/L for BuOH. Small concentration differences are accounted for by density differences in the feeds. %GE and gasification rate were calculated along with error estimation from replicate runs as before. The results are also given in Table 5.3 above. Runs 11-16 were run with pure alcohol in the carbon stream. Runs 17-19 were run with each alcohol diluted with water in the carbon stream so that reaction order, n, could be determined as described in section 5.7. Note the run number was for bookkeeping and not the order in which the experiments were performed and each data point is the average of replicate runs.

5.7 TEMPERATURE & CONCENTRATION PROFILE AND ESTIMATION OF E_A

In order to model reaction rate as a function of temperature, the temperature of the reacting stream must be known as a function of distance down the reactor. Figure 5.3 shows the polynomial fit of the temperature profiles at 1.2 s residence times for the runs at a furnace

temperature of 720° in Table 5.3. Both BuOH and EtOH had essentially the same temperature profile for each corresponding run as described in section 5.4. In Figure 5.3, runs 12 and 17 had the same temperature profile because, as described in section 5.5, the temperature of the reacting fluid was dependent on the furnace temperature and the flow rate of each stream and not the composition of the carbon loading stream. Although not in Figure 5.3, runs 14 and 18 as well as 16 and 19 also had the same temperature profiles. So for the nine runs for each species in Table 5.3, there are 6 unique temperature profiles and 3 duplicates. The duplicate temperature profiles are used to calculate n. Obviously, increasing the furnace temperature from 720° to 750° to 780° lifted the temperature curves at each respective concentration. For each curve, the correlation was $R^2 > .98$. As described above, a "chimney effect" was observed at every run. In addition to the polynomial fit, the actual data points are also shown.

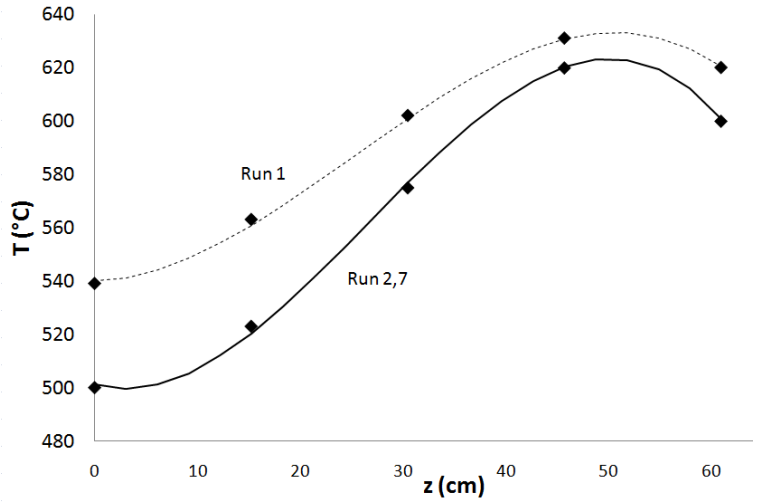

Figure 5.3. Fluid temperature profile τ = 1.2 s for runs at 720° furnace temperature in Table 5.3.

As mentioned above, the pairs of runs 17 and 12, 18 and 14, 19 and 16 have the same temperature profile but different concentrations and can be used to solve for reaction order, n. Using runs 17 and 12 as an example: $\frac{Rate_{17}}{Rate_{12}} = \frac{k_{17}C_{17}^n}{k_{12}C_{12}^n} = (\frac{C_{17}}{C_{12}})^n$ because k_{17} and k_{12} are the same because of identical temperature profiles. The same can be done for runs 18/14 and 19/16 to determine n.

After determining n, predicted concentration profiles were generated as a function of distance, z, down the reactor. In the Arrhenius equation above, *T = T(z)* is the descriptive temperature profile of each respective run (third order polynomial, $R^2 \geq .98$). So from $\frac{-d[C]}{dt} = \frac{C_i - C_f}{\tau} = Aexp(\frac{-E_a}{RT})C^n$, then, $C_i(z) = C_{i-1}(z) - A\Delta t \cdot \exp[\frac{-E_a}{R \cdot T_i(z)}]C^n$, where *i* is numerical place keeper, gives the predicted concentration profile as a function of distance down the reactor. Knowing the concentration at the end of the reactor, $C_{f,observed}(L) = C_i(1\text{-}GE)$, makes it possible to solve for the pre-exponential factor, A, and the activation energy, E_a by minimizing the differences between $C_{f,predicted}$ and $C_{f,observed}$ in all 9 runs for each species.

It should be noted that A is not independent of E_a. Therefore, A was chosen as an appropriate scaling factor so that exponential term would describe the variation in k across the temperature profiles shown in Figure 5.3 to agree with observations. From above, $k = Aexp\left(\frac{-E_a}{RT}\right)$. Figure 5.4 shows the concentration profile for a representative number of runs for EtOH. Here, runs 12 and 17, 16 and 19 have the same temperature profile. The lines represent the predicted concentration profile based on E_a, A, and n and the points represent the observed initial and final concentration. BuOH showed a similar concentration profile.

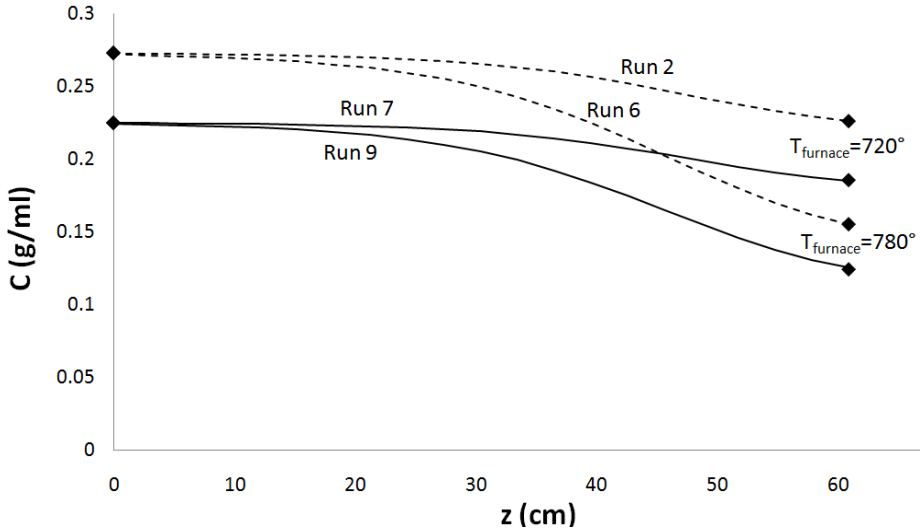

Figure 5.4. Concentration profile of representative runs of EtOH of predicted values (lines) and observed values (points) during high flow intrinsic rate measurements from Table 5.3.

Table 5.4 gives estimations of the three Arrhenius parameters for both alcohols based on this analysis. The same procedure described above can be used to estimate these parameters for any carbon feed. Good estimates of E_a, n, and A for a large number of feeds are important for advancing SCWG technology and sizing larger reactors. For example, if a certain annual quantity of feed is available for gasification, and the Arrhenius parameters for that feed are known, a reactor can be appropriately sized to handle such a throughput.

	E_a	n	A
EtOH	147 kJ/mol	0.80	$5 \cdot 10^6 (g/L)^{0.2}/s$
BuOH	137 kJ/mol	0.74	$1 \cdot 10^6 (g/L)^{0.26}/s$

Table 5.4. Arrhenius parameters E_a, n, and A for EtOH and BuOH.

Looking at Table 5.4 and Figure 5.2, EtOH has a larger activation energy than BuOH but also gasified more efficiently at every residence time. This appears to be inconsistent, but is due to a variety of effects. First, both the reaction order (n) and pre-exponential scale factor (A) are larger for EtOH. This requires a larger magnitude of E_a to predict temperature behavior. Also, higher oxygen content in EtOH will decrease the energy density of its vapor product, and the results are consistent with a net energy balance. See section 5.8 for more on vapor product composition.

To show the accuracy of the Arrhenius model, Figure 5.5 shows the observed final concentration against the predicated final concentration for each run with each species at the reactor exit with 95% confidence intervals. Observed final concentration is found by: $C_{f,observed} = C_i(1\text{-}GE)$. Predicted final concentration is found using the temperature profile (a representative number are shown in Figure 5.3) with Arrhenius parameters described above and z = L. When plotted, the points in Figure 5.5 are compared against the y = x line representing a perfect model fit. Correlation values are: for EtOH, $R^2 = 0.85$, for BuOH, $R^2 = 0.90$. The maximum error observed was 14% (EtOH) and 10% (BuOH). The average error was 5% (EtOH) and 6% (BuOH).

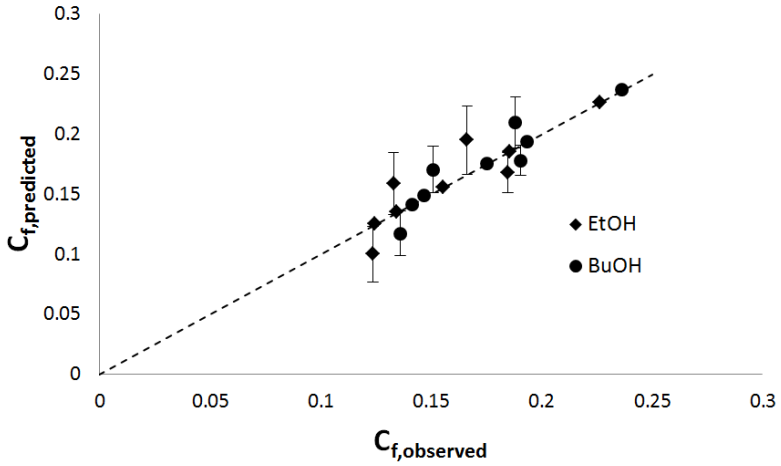

Figure 5.5. Predicted against observed final concentrations for EtOH and BuOH with 95% confidence intervals and the y = x line in the background.

5.8 EFFECT OF FEED ON VAPOR PRODUCT COMPOSITION

Gasified vapor (valuable product mixture) is collected from the high pressure liquid/vapor separator for GC analysis. All of the water downstream of the cooling coil is condensed and drained out the bottom of the separator leaving a clean, dry vapor product. Figure 5.6 shows the composition of the vapor product as mole fractions from GC analysis for feeds of EtOH and BuOH. Figure 5.6(a) and 5.6(b) compares EtOH and BuOH, respectively, at long and short residence times. Figure 5.6(c) compares EtOH and BuOH at short residence times. In Figure 5.6, "long" and "short" residence time data was taken at τ = 15 s and τ = 1.2 s, respectively. When $\tau \geq 15$ s, %GE is maximized; when $\tau \leq 1.2$ s, gasification rate is maximized (see Table 5.2 and Figure 5.2).

Figure 5.6 gives insight as to how the composition of the feed stream effects the composition of the vapor product. By weight, EtOH is 52% C, 13% H, 35% O; BuOH is 65% C, 13% H, 22% O. Most of the oxygen present in the organic feed is incorporated in CO_2 molecules in the product (the rest is in CO). Because of this characteristic, SCWG of EtOH is less endothermic than BuOH (Venktasamy 2011). From Table 5.2, EtOH gasified more efficiently than BuOH at all residence times, however, the vapor product of EtOH is has lower energy

density because of higher composition of CO_2 and lower composition of CH_4. Both species produced similar amounts of H_2. A previous report details the effect of feed oxidation state on vapor product composition (Venktasamy 2011).

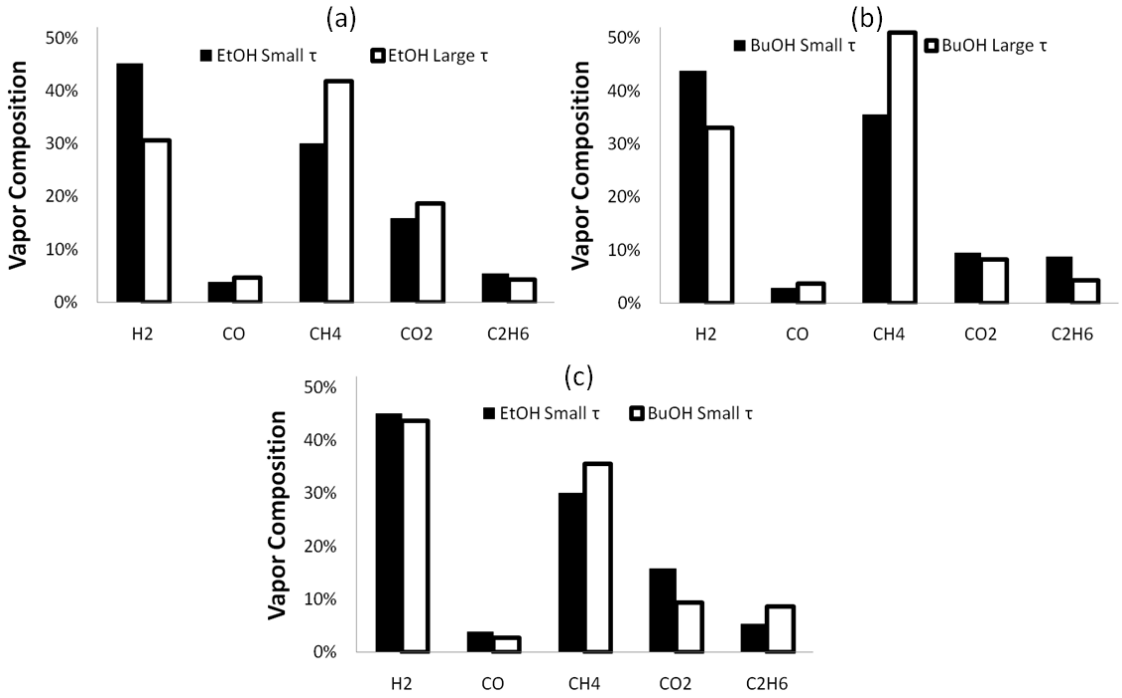

Figure 5.6. Comparisons of vapor product composition of EtOH and BuOH at long and short residence times.

5.9 CONCLUSIONS

SCW gasification of ethanol and butanol were explored over a range of residence times from 0.7 – 34 seconds. Maximum gasification rates occurred when $\tau \leq 1.2$ s, corresponding to high Reynolds numbers, turbulent flow, and effective axial mixing, allowing observation of intrinsic reaction rate. Additional experiments were performed under turbulent, plug flow conditions at various concentrations and temperatures. Arrhenius parameters of the gasification reaction were estimated for ethanol and butanol with intrinsic rate data. The gasification rates observed at turbulent conditions are the highest SCWG rates ever reported. Such high gasification rates present the potential for SCWG as a viable, high throughput process.

6. Investigation of Enhanced Downstream Separations for Carbon Capture

6.1 SUMMARY

The separation of a supercritical mixture of nitrogen and carbon dioxide is explored at pressures from 10 to 31 MPa and temperatures of -5° and 23°C. Nitrogen is used as a model compound for valuable fuel gases (H_2, CH_4) produced during SCWG. An "ideal interface" resembling that between water and air at ambient conditions does not form. Rather, a concentration gradient is observed. Nitrogen mole fraction increases in the positive vertical direction and approaches unity near the top of the pressure vessel. Carbon dioxide mole fraction increases in the negative vertical direction and approaches unity near the bottom. This concentration gradient is the basis of an effective separation. As the system pressure increases and/or the system temperature decreases, this density driven concentration gradient becomes less pronounced. Consequently, the separation effectiveness is also increased with increased pressure and decreased temperature. The time to achieve maximum separation is quantified, and found to decrease with increasing pressure. At the conditions studied, nitrogen is a supercritical fluid as a pure component while carbon dioxide is a liquid as a pure component, however the mixture is considered supercritical. The observation of a concentration gradient, and thus separation, is due to nonhomogeneities in the supercritical fluid mixture with density driven concentration gradients. Preliminary experiments were also performed with additional binary systems: CO_2/H_2, CO_2/CH_4, and CO_2/Air, all of which behave similarly to the CO_2/N_2 system. This kind of separation has applications in continuous processing of pressurized gasification products, other biomass refinery operations, and in the natural gas industry.

6.2 ORIGINAL EXPERIMENTAL SETUP WITH ULTASOUND TECHNOLOGY

The original experimental setup was intended to utilize ultrasound technology to detect a liquid/vapor interface between liquid CO_2 and a vapor phase of mostly N_2 and smaller amounts

of CO_2 (in equilibrium with its vapor). The original experimental setup is shown in Figure 6.2 below. Because the pressure in these experiments far exceeds the saturation pressure of CO_2 (a function of temperature), it seemed plausible that a high pressure system with CO_2 would establish a vapor/liquid equilibrium (VLE) that could be the basis of an effective separation. The phase boundary was to be detected by an ultrasonic probe operating in pulse-echo mode.

Figure 6.1 presents preliminary results using ultrasound to measure the height of a VLE phase boundary. The data in the figure was generated using the binary system of water and air at ambient conditions, which is known to create a distinct phase boundary. The figure shows that the ultrasonic probe operating in pulse echo mode measures the time of flight (the time for a sound wave to hit the phase boundary and return to the probe for detection) and use that measurement to accurately predict the liquid phase height. These preliminary experiments were performed in the same high pressure phase equilibrium separator (HEPS) that is used for subsequent experiments reported here including experiments with CO_2 and N_2 at high pressure.

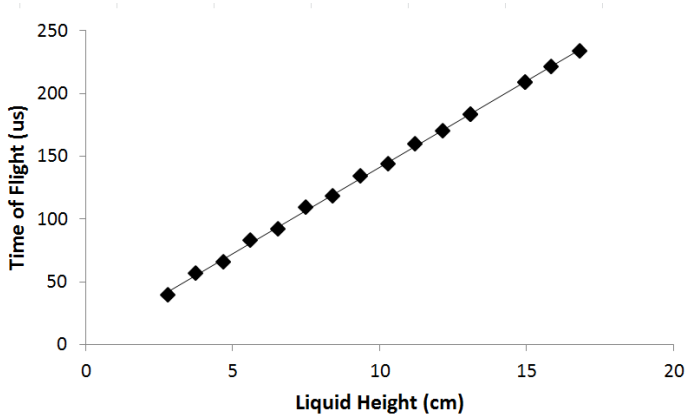

Figure 6.1. Results of ultrasonic sensing of VLE interface with water/air system at ambient conditions. Such positive results were not observed with CO_2/N_2 system.

While the data in Figure 6.1 was collected at ambient conditions, an experimental setup had to be created to perform experiments at high pressure. Experiments were done in an isolated high HEPS made of stainless steel. The cylindrical separator had an inner diameter of 8.3 cm and inner height of 18 cm for a volume of 950 cm^3. Additional plumbing includes tubing

with 0.38 cm inner diameter with compression tube fittings. The separator was plumbed to a syringe pump (ISCO 260D) which was plumbed to high pressure reservoir tanks with 99.9% purity so that individual species could be pumped from the syringe pump through a one way valve into the HEPS. By monitoring conditions in the syringe pump (i.e. temperature, pressure), the amount of each species pumped into the separator was known and is described below. Here "U" indicates an ultrasonic probe operating in pulse-echo mode to detect the phase boundary. The schematic is shown in Figure 6.2.

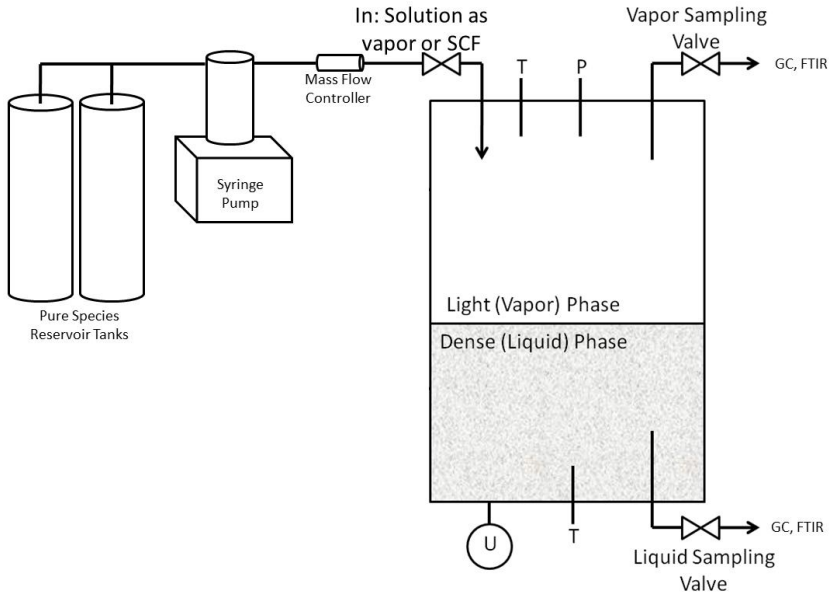

Figure 6.2. Original setup of HEPS system for investigating high pressure phase equilibrium with CO_2.

The results obtained with ultrasonic detection of a phase boundary with the water/air system were not able to be duplicated with the pressurized CO_2/N_2 system. It was concluded that the CO_2/N_2 system did not establish traditional VLE with a distinct phase boundary and further investigation of the system was needed before an effective separation strategy could be incorporated.

6.3 REVIEW OF HIGH PRESSURE CARBON DIOXIDE PHASE EQUILIBRIUM

Multi-species phase equilibrium with carbon dioxide (CO_2) has been explored in the literature. At temperatures below the critical temperature (31°C) and pressures above the saturation pressure (a function of temperature), CO_2 can exist as a liquid. Therefore, in vapor-liquid equilibrium of a binary system at sufficiently high pressures, CO_2 can exist primarily in the dense (liquid) phase. The purpose of this investigation is to observe CO_2 as the dense phase in a binary system including nitrogen (N_2/CO_2).

Several reports have estimated thermodynamic variables of interest for the N_2/CO_2 system. Table 6.1 tabulates the critical point estimate of the system as a function of mole fraction of CO_2 from several sources. Figure 6.3 presents the data in graphical form. Some of the experiments presented below are done at overall mole fractions of 0.5:0.5 N_2:CO_2. Based on a simple regression, the critical point of the system at 50% mole fraction of both CO_2 and N_2 is -9°C and 9.8 MPa. While the conditions investigated in this study exceed this estimated critical point indicating that the system should be a supercritical fluid mixture, there is still an observable separation. This separation is due to a density driven gradient and explained further in sections 6.7 – 61.10.

X_{CO2}	T_C (°C)	P_C (MPa)	Reference
1	30.97	7.374	Poling 2007
0.95	27.12	8.113	Goos 2010
0.9	22.51	8.77	Goos 2010
0.8	12	10.224	Goos 2010
0.447	-15.35	9.364	Esper 1989
0	-146.95	3.398	Poling 2007

Table 6.1. Critical Temperature and Pressure of N_2/CO_2 mixture as a function of CO_2 mole fraction.

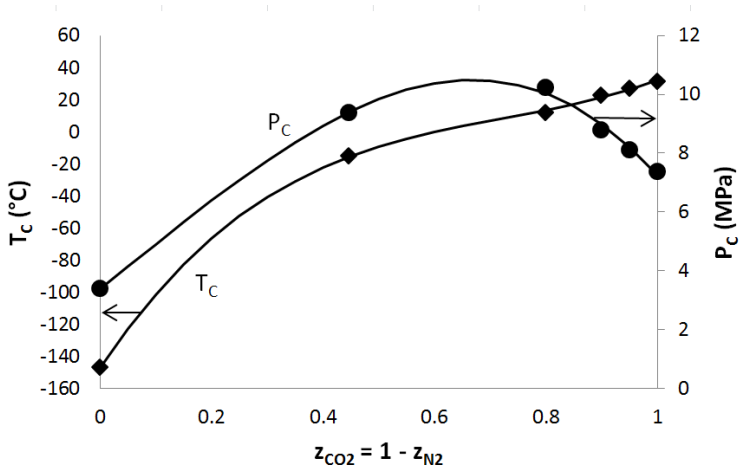

Figure 6.3. Critical Temperature and Pressure of N_2/CO_2 mixture as a function of CO_2 mole fraction.

With the critical point of the CO_2/N_2 mixture known, Li (2008) reviews vapor liquid equilibrium (VLE) of CO_2/N_2 mixtures below the mixture critical point (see Figure 6.3). Such VLE exists at $-20° \leq T \leq 15°C$; $2.35 \leq P \leq 13.95$ MPa; $0.85 \leq x_{CO2} \leq 1$; and $0.49 \leq y_{CO2} \leq 1$. The temperature and pressure in this study exceed this range where VLE occurs, consistent with the established critical point above.

The results in sections 6.7 – 6.10 describe a nonhomogeneous supercritical fluid mixture of CO_2 and N_2 with density driven concentration gradients. Most supercritical fluids and supercritical fluid mixtures are thought to be homogeneous. However, for a binary mixture, the term supercritical is more arbitrary than for a pure substance. Further, CO_2 and N_2 have no chemical or molecular interactions between each other so it makes sense that a separation may be possible.

Ree (1986) computed the detonation properties of two explosives using reliable statistical mechanical theories and realistic intermolecular potentials as a way to analyze data on mixtures at high pressures. The calculations shows that the detonation products of explosives containing N_2, CO_2, and H_2O can separate into N_2-rich and N_2-poor fluid phases producing a "gas-gas phase separation". The authors made a separate study on binary mixtures

including N_2/CO_2. The results of this study show that a fluid phase separation may occur at sufficiently high pressures and temperatures, however this reference only included theories and simulations instead and experiments were not performed to confirm calculations.

6.4 CURRENT CARBON CAPTURE TECHNOLOGY

In a power plant setting, there are three main technology options for CO_2 separation: post-combustion capture, pre-combustion capture, and oxy-fuel combustion capture (Li 2008). Post-combustion capture means capturing CO_2 from the flue gases produced by the combustion of fossil fuels and biomass in air. It is a downstream process, in which the CO_2 in flue gas at near atmospheric pressure is typically removed by a chemical absorption process using absorbents such as alkanolamines. Pre-combustion capture is to separate the fuel-bound carbon before the fuel is combusted. This involves a reaction between fuel and oxygen to primarily produce synthesis gas, which contains carbon monoxide and hydrogen. The carbon monoxide reacts with steam in a catalytic reactor, called a shift converter, to give CO_2 and more hydrogen. CO_2 is then separated, usually by a physical or chemical absorption process. Oxy-fuel combustion capture means capturing CO_2 from the flue gases produced in oxy-fuel combustion. The oxy-fuel combustion is the combustion taking place in a no-nitrogen environment, resulting in a flue gas mainly consisting of H_2O and CO_2. The technical-economic comparison of the three CO_2 capture technologies is still under way for large-scale industrial applications. A preferable technology would involve an equilibrium separation because there would be no required energy input or potentially costly absorbent to achieve the separation.

A review article Yang (2008) summarizes the progress made in CO_2 separation and capture research and engineering. Essentially all of the advancements in the area have come from technologies such as absorption, adsorption, membrane separation, and to a lesser extent newer concepts such as chemical-looping combustion and hydrate-based separation. Such

separation technologies are often hindered by energy and financial input costs. Using equilibrium separations have many advantages over these other separation technologies because it offers a relatively cheap, energy efficient, large volume separation process.

6.5 IMPROVED EXPERIMENTAL SETUP AND OPERATING PROCEDURE

It was decided to continue investigation of potential separations in the CO_2/N_2 fluid mixture. Because the mixture does not product traditional phase boundaries, the ultrasonic probe was removed and the HEPS was plumbed to include ports for composition sampling. The experimental setup is shown schematically in Figure 6.4. From Figure 6.4 it is seen that the HEPS has four sampling ports designated as follows: (1) top, (2) high (1/3 of the height below top); (3) low (1/3 of the height above bottom); (4) bottom. The four sampling ports gave composition samples at four locations in the HEPS which was important since a concentration gradient is observed as described below.

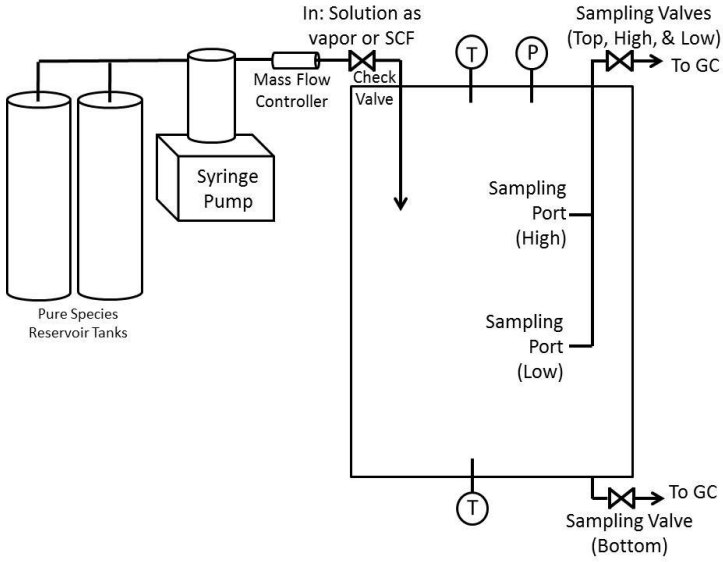

Figure 6.4. Schematic of HEPS and experimental setup.

Prior to each experiment, the HEPS was first flushed out with CO_2 to remove any air. Then pure CO_2 was pumped into the separator. For each experiment, the amount of CO_2 and N_2 was determined from experience to obtain the desired pressure. The overall mole fraction of

each species was kept at 0.5 for each experiment unless indicated otherwise. For any separation to occur in the HEPS, the pressure needed to be greater than the saturation pressure of CO_2 at the given temperature. The saturation pressure of CO_2 as a function of temperature is well known. These values were in agreement with the pressures observed in the HEPS during loading at a given temperature. These observations were consistent with formation of a dense phase at high pressures. After pumping in CO_2, N_2 was pumped in a quantity to achieve equimolar concentration with CO_2. After filling, the HEPS was allowed to sit undisturbed for several hours to ensure equilibrium was reached. In experiments done at reduced temperature, the HEPS was allowed to equilibrate in a freezer. Composition samples were taken using gas chromatography (GC) at each of the four ports.

6.6 QUANTIFYING MASS LOADED AND SAMPLING

During loading of the HEPS, in the syringe pump (i.e. temperature, pressure) were carefully monitored. The amount of each pure species pumped into the separator was known from observed volume changes and density estimation by an equation of state for pure species. Preliminary data was collected using the Peng-Robinson equation of state. To determine the accuracy of that equation of state, a comparison was done with a reference equation of state for CO_2 (Span 1994) and for N_2 (Span 1998). Because each reference equation of state was designed specifically for each respective species, they were used in results reported here. However, Table 6.2 below shows that there is little difference in density calculations between each equation of state in the range of temperatures and pressures observed in the syringe pump for CO_2. Comparison of each equation of state for N_2 also showed small differences at the conditions in the syringe pump. However, it should be noted that the Peng-Robinson equation of state and the reference equations of state do increase in deviation as pressure increases much past 15 MPa for CO_2 and 25 MPa for N_2.

		ρ (g/cm^3)		
T (K)	P (MPa)	PR EOS	Ref EOS	Difference
290	4	0.102	0.100	1.8%
300	4	0.094	0.092	2.0%
290	5	0.151	0.148	1.7%
300	5	0.132	0.128	2.4%
290	6	0.772	0.821	6.0%
300	6	0.187	0.182	2.5%

Table 6.2. Comparison of density estimations between the Peng Robinson equation of state (PR EOS) and the reference equations of state (Ref EOS) for CO_2.

To show separation within the HEPS, composition samples were analyzed with gas chromatography (GC). One advantage of using GC for analysis is that a small amount of vapor is needed for analysis, thus the system remains essentially undisturbed. GC analysis requires <1 ml of vapor (at ambient pressure), which is an insignificant amount of vapor relative to that in the system, almost 1 liter of highly pressurized vapor. For most experiments, composition samples are taken from four places throughout the separator: the top, high port (6 cm below the top), low port (6 cm from the bottom), and the bottom of the HEPS. Some experiments only required sampling from one or two ports. Each experiment reported is an average of duplicate samples ($n_{samp} \geq 2$) and duplicate HEPS loadings ($n_{load} \geq 2$) to improve accuracy and evaluate precision. The maximum variance observed was less than 4% of the average. Such small variances are due to the consistency in the HEPS loading procedure as well as the composition sampling procedure. Additionally, the experiments done here are done in batch mode so conditions in the HEPS are easily controlled and repeatable.

6.7 RESULTS: PRESSURE EFFECTS

Figure 6.5 shows the raw sampling data from the HEPS with N_2 and CO_2 in equilibrium from 10 MPa to 29 MPa. The overall mole fraction, z, of each species in each experiment is 0.5. Equilibrium temperature was held at 23°C ± 0.5° for each experiment. For reference, the saturation pressure of CO_2 at 23°C is 6.1 MPa. As described above, the overall mole fractions are found by estimating the quantity of each species pumped into the HEPS using reference

equations of state. The four sample labels indicate the location in the HEPS that each sample was taken. "Top" and "bottom" indicate the top and bottom of the HEPS. "High" indicates the sample taken 6 cm below the top (1/3 of the HEPS height from the top) and "low" indicates the sample taken 12 cm below the top (1/3 of the HEPS height from the bottom). Figure 6.5 shows a concentration gradient at each pressure, but also shows an increasingly effective separation between the two species with increasing pressure. These are promising results because several processes in a biorefinery might operate at pressures well above 29 MPa, which from Figure 6.5, would produce close to perfect separations.

Figure 6.5 reveals that a homogeneous less-dense phase and a homogeneous more-dense phase are not separated by an ideal interface, as would be expected during vapor-liquid equilibrium. The CO_2/N_2 mixture is a *non-homogeneous supercritical fluid* and it exhibits a *density driven concentration gradient*. This is consistent with the literature that VLE in the CO_2/N_2 system does not occur when $T \geq 15°C$ and $P \geq 14$ MPa (Li 2008), but that a separation into a N_2 rich and N_2 poor phase is possible even at temperatures above the point of VLE (Ree 1986).

The composition samples from the top of the HEPS provide insight into the amount of CO_2 in the less-dense phase. It is supported in that, even at the highest pressure, measureable CO_2 appeared in the sample taken at the top. However, as pressure increases, the mole fraction of CO_2 in the less-dense phase approaches zero, suggesting potential as a separation technology. The composition of samples taken at the bottom of the HEPS signifies the dense phase contains nearly neat CO_2. At the highest pressure, no detectable amount of N_2 was observed in the samples taken at the bottom.

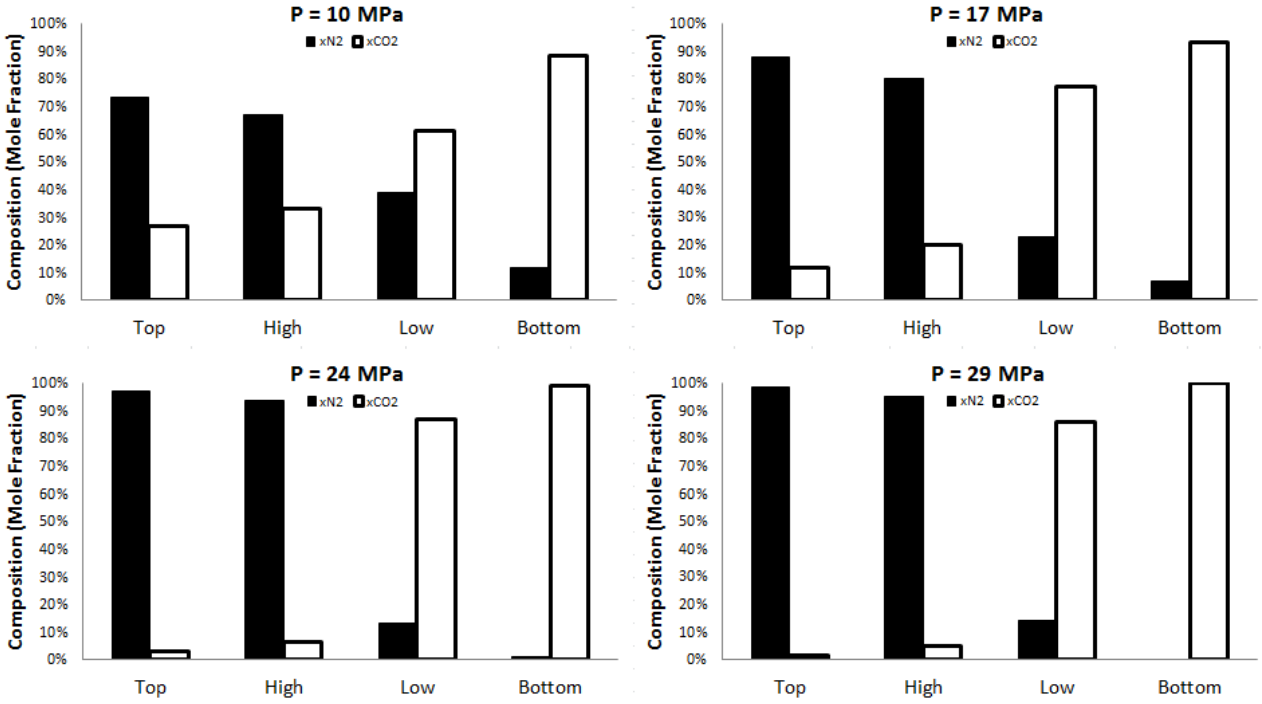

Figure 6.5. Effect of pressure on the separation of CO_2 and N_2 in the HEPS. T = 23°C; $z_{CO2} = z_{N2} = 0.5$.

The data in Figure 6.5 show that, despite the absence of an ideal interface, the presence of a density-driven concentration gradient can provide the basis for an effective separation of CO_2 and N_2. The data in Figure 6.5 also supports the hypothesis that separation increases with pressure. Even though the fluid is supposedly a supercritical fluid, the nitrogen and carbon dioxide molecules have little interaction and the carbon dioxide appears to behave in some ways like a dense liquid with a vapor pressure. This observation of increasing separation with increasing pressure is consistent with the fact that the vapor pressure of CO_2 is constant with constant temperature, thus as pressure increases, the effectiveness of the separation should also increase.

Figure 6.6 more clearly shows the increased effectiveness of separation between N_2 and CO_2 in the HEPS with increasing pressure. Each data point in the dense phase in Figure 6.6 was taken from the bottom of the HEPS after equilibrium was reached, while each data point in the light phase was taken from the top of the HEPS. Overall mole fractions were maintained at 0.5

for each species and temperature of the HEPS was maintained at 23°. The trends, represented by dotted lines in Figure 6.6, indicate as pressure is increased beyond 30 MPa while temperature and overall mole fractions are held constant, the composition of CO_2 in the light phase approaches zero and the composition of CO_2 in the dense phase approach 1.

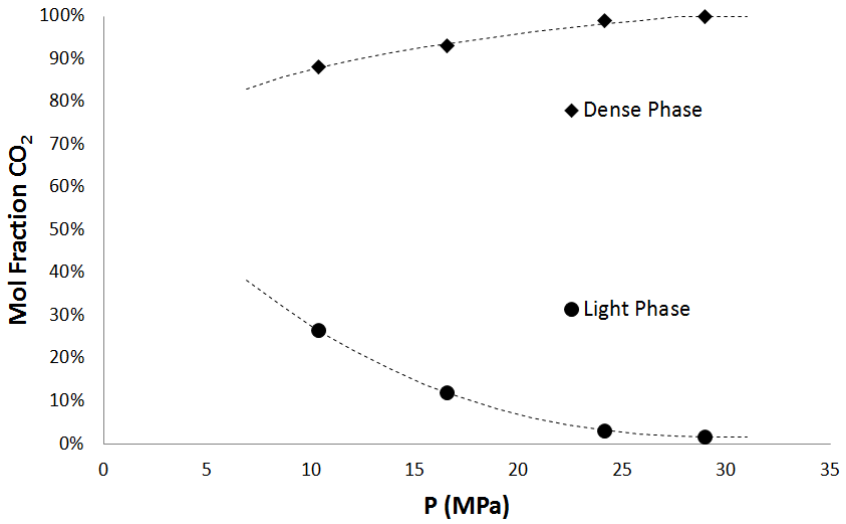

Figure 6.6. Mole fraction of CO_2 in the light and dense phases as a function of pressure demonstrating effectiveness of separation. T = 23°C; $z_{CO2} = z_{N2} = 0.5$.

6.8 RESULTS: TEMPERATURE EFFECTS

Figure 6.7 shows a comparison of the composition samples of N_2 and CO_2 in the HEPS at different equilibrium temperatures: -5° and 23°C. Using simple regression in Figure 6.3, it is seen that even at a temperature of -5°, the N_2/CO_2 fluid mixture is still above the mixture's critical point. The pressure was held constant at 13 MPa and overall mole fractions of each species were 0.5. Maintaining pressure at different temperatures required loading the cold HEPS with a higher mass of each species. For reference, the amount of mass loaded into the HEPS chilled to -5° created a pressure of 31 MPa when allowed to warm to 23°. Figure 6.7 indicates that the chilled HEPS showed a greater concentration of N_2 in the light phase and a greater concentration of CO_2 in the dense phase, thus a better separation. An explanation, similar to the explanation about pressure effects, is that CO_2 behaves somewhat independently

of N_2 and exhibits a vapor pressure that decreases with decreasing temperature, which explains a more pronounced separation. As before, the CO_2/N_2 mixture is acting as a *non-homogeneous supercritical fluid.* A density driven concentration gradient was still evident at both temperatures, and as described above, diminishes as pressure is increased.

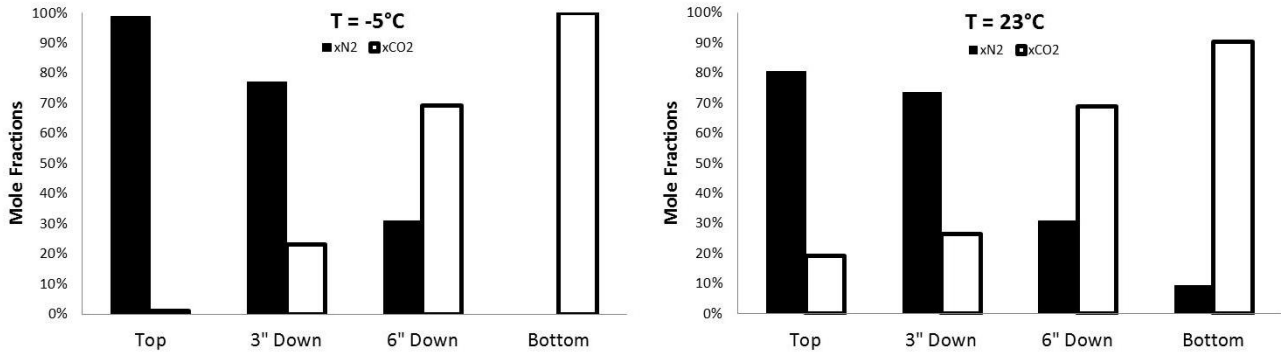

Figure 6.7. Equilibrium mole fractions in the HEPS at -5° & 23°. P = 13 MPa; $z_{CO2} = z_{N2} = 0.5$.

6.9 RESULTS: APPROACH TO EQUILIBRIUM

The rate of approach to equilibrium of the CO_2/N_2 system is explored in Figure 6.8. The experiments reported above were all performed in batch mode and allowed to come to equilibrium. However, design of an HEPS to be operated in continuous mode requires quantification of the rate of approach to equilibrium. To accomplish this, the HEPS was loaded using the same method as previous experiments, and allowed to equilibrate. Before sampling, the HEPS was inverted to sufficiently agitate the fluid inside. Thus, the top of the HEPS became the bottom and vice versa. After agitating, the HEPS was left to sit for a specified amount of time before a sample was taken. Figure 6.8 shows the composition of these samples in comparison to a control, which was allowed to come to full equilibrium. Figure 6.8a was sampled at 31 MPa and Figure 6.8b was sampled at 15.5 MPa, thus allowing observation of the effect of pressure on the approach to equilibrium. The samples in Figure 6.8 visually show the agitated system equilibrating with the dense phase (primarily CO_2) settling below the light phase.

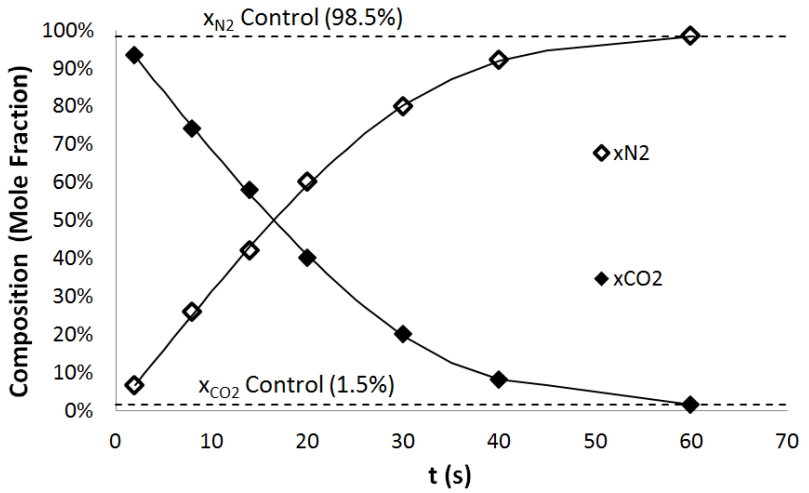

Figure 6.8a. Approach to equilibrium in the HEPS. T = 23°C; P = 31 MPa; $z_{CO2} = z_{N2} = 0.5$. Samples were taken from the top after HEPS had equilibrated for specified time after complete agitation.

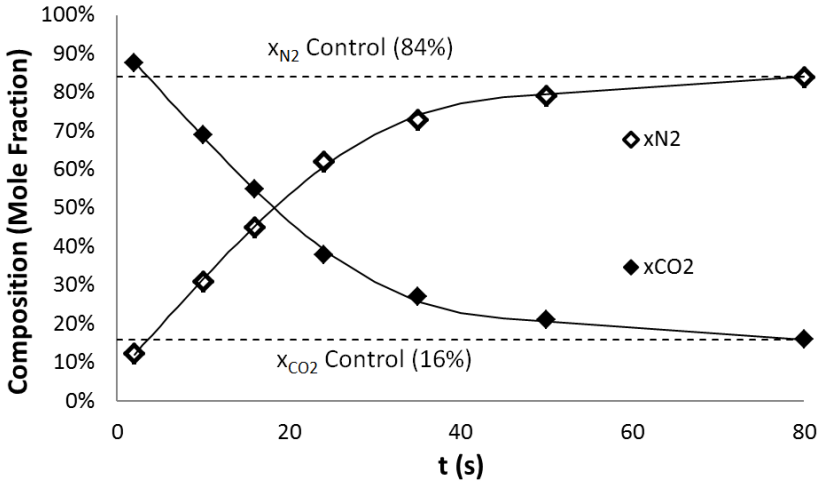

Figure 6.8b. Approach to equilibrium in the HEPS. T = 23°C; P = 15.5 MPa; $z_{CO2} = z_{N2} = 0.5$. Samples were taken from the top after HEPS had equilibrated for specified time after complete agitation.

It should be noted that a pressure drop up to 3% was observed during inversion (agitation) of the HEPS. This can be explained by the fact that inverting the HEPS induces movement of the fluid due to the observed density driven concentration gradient. Fluid in motion produces less pressure than if stagnant (Bernoulli's principle). The pressure would always return to its initial value indicating that equilibrium had been re-established.

Figure 6.8a indicates that complete equilibrium in the system at 31 MPa occurred in 60 seconds. Equilibrium in this case refers to establishing equilibrium concentration gradients

rather than a vapor-liquid equilibrium. The HEPS was already at thermal equilibrium. After 40 seconds, the system had reached 93% of equilibrium concentration conditions. Figure 6.8b indicates that complete equilibrium in the system at 15.5 MPa occurred in 80 seconds. After 50 seconds, the system reached 94% of equilibrium concentration conditions. Figure 6.8 suggests that increasing pressure causes a more rapid approach to equilibrium. This is not surprising, as Figure 6.5 shows that increasing pressure also causes a better separation. All of the data presented in this report was taken in a batch mode, however the information presented in Figure 6.8 is useful when designing a continuously operated HEPS. It appears that operating a continuous HEPS at higher pressure reduces the average residence time needed to achieve maximum separation. For example, in a continuous HEPS operating at 31 MPa or higher, an average residence time of 60 seconds should be enough to achieve maximum separation.

6.10 RESULTS: LONG TIME SAMPLING

Because the fluid mixture in the HEPS is considered a supercritical fluid (see section 6.3), sampling at long time was done to assure that the non-homogeneous supercritical fluid does not return to a homogeneous state. The HEPS is filled to 31 MPa with overall mole fraction of 75% CO_2 and 25% N_2 and allowed to sit undisturbed for 6 days with intermittent sampling during that time. As described above, using the GC for sampling created minimal disturbance to the HEPS. The results of the long time experiment are given in Figure 6.9. The results show that the separation in the HEPS is essentially permanent. There was a small change in the concentration of the high and low sampling ports, but the top and bottom samples, which represent the true separation potential, remained the same over the 6 days of sampling. This result is not surprising because the separation is based on the density driven concentration gradient, which was not expected to change at long times. The indication that the separation is permanent is promising when designing a HEPS for use in continuous processes.

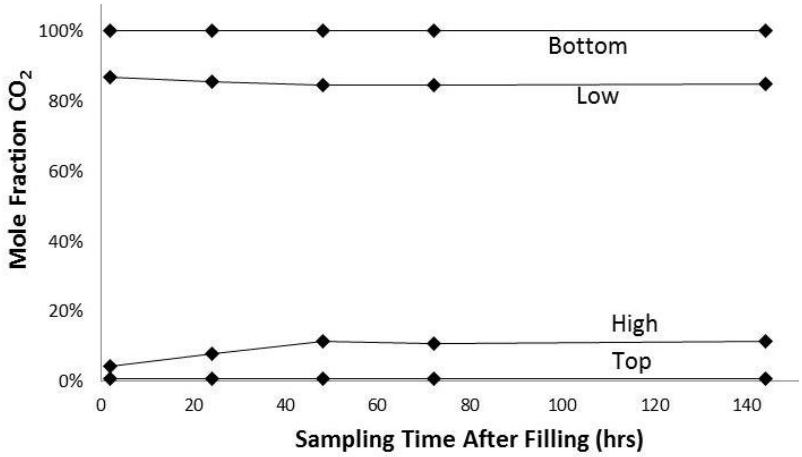

Figure 6.9. Long time results indicating that the CO_2/N_2 nonhomogeneous supercritical fluid does not return to a homogeneous state (i.e. separation is lasting). T = 23°C; P = 31 MPa; z_{CO2} = .75; z_{N2} = .25.

6.11 INTERACTION OF CO_2 AND AIR (TERTIARY SYSTEM)

The results with the CO_2/N_2 binary system were very promising and offer many potential applications in continuous processing of pressurized gasification products, biomass refinery operations, and in the natural gas industry. Based on these potential applications, several experiments were performed with the tertiary system of CO_2 and air (N_2 and O_2). These experiments were performed because the CO_2/Air fluid mixture system might have even more applications that the CO_2/N_2 system. The results are summarized in Figure 6.10. The results in figure 6.10 are from a mixture of 60% CO_2 and 40% air on a molar basis. The HEPS was loaded in the same way as before using air instead of N_2. The critical point of a mixture of CO_2 and air is very similar to that of a mixture of CO_2 and N_2 as shown in Figure 6.3. The critical point of pure air is T_C = -141°C and P_C = 3.8 MPa. The CO_2/Air fluid mixture is a nonhomogeneous supercritical fluid with a density driven concentration gradient at the given conditions.

Even though air is composed of O_2 and N_2 making the CO_2/Air mixture a tertiary mixture, it is displayed in Figure 6.10 as though it was a binary mixture because there was essentially no separation of the oxygen and nitrogen components (i.e. air was treated as a single species). As with all other runs, the results were replicated to verify accuracy. As with the CO_2/N_2 system,

the separation appears to equilibrate quickly and remain permanent. The results in Figure 6.10 suggest that the CO_2/Air system behaves very similarly to the CO_2/N_2 system. Thus data from the CO_2/N_2 system in sections above can be used as a rough approximation as to how the CO_2/Air system will behave.

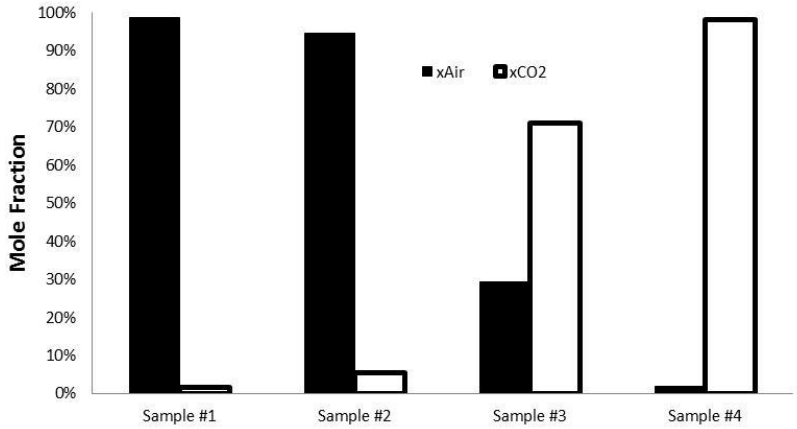

Figure 6.10. Results with CO_2/Air. P = 29 MPa; T = 23°C; z_{Air} = 40%; z_{CO2} = 60%.

6.12 PELIMINARY SEPARATION DATA WITH CO_2/CH_4 & CO_2/H_2

Using the same procedure as described with the CO_2/N_2 system, preliminary data on two other binary systems were taken: CO_2/CH_4 and CO_2/H_2. The data collected on the CO_2/N_2 system is very useful; however experimental data with CH_4 and H_2 are much more applicable to implementation of high pressure separations in a biorefinery. Like N_2, CH_4 and H_2 are both supercritical fluids as pure species at the conditions in the investigation. The critical points of these species are as follows: CH_4 (T_C = -83°C, P_C = 4.6 MPa) and H_2 (T_C = -240°C, P_C = 1.3 MPa). While the data with CH_4 and H_2 is only preliminary and has not been replicated thoroughly enough for publication, the same trends as the data with N_2 are observed. That is, both binary systems of CO_2/CH_4 and CO_2/H_2 produced a nonhomogeneous supercritical fluid mixture with density driven concentration gradients. Figure 6.11 shows this concentration gradient for both systems, each at 23° and 20 MPa and equal overall mole fractions. Figure 6.12 includes separation data from all four systems as a function of pressure for comparison with the CO_2/N_2

system. All of the data in Figure 6.12 was collected at equal overall mole fractions ($z_i = z_{CO2} = 0.5$) It is encouraging to see that preliminary data suggests that the CO_2/CH_4 and CO_2/H_2 systems might produce even better separations at the same pressures than CO_2/N_2.

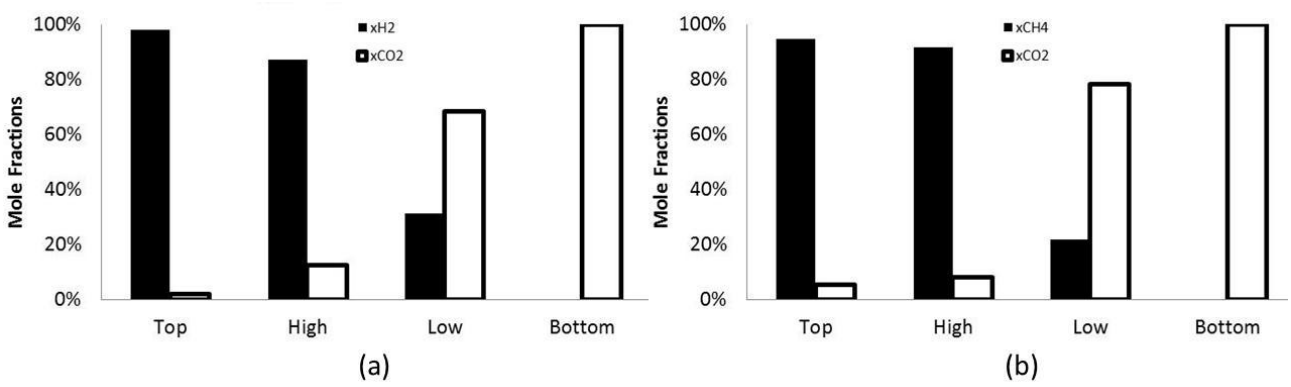

Figure 6.11. Preliminary data showing density driven concentration gradient in two binary systems: (a) CO_2/H_2 and (b) CO_2/CH_4. T = 23°C, P = 20 MPa, $z_i = 0.5$.

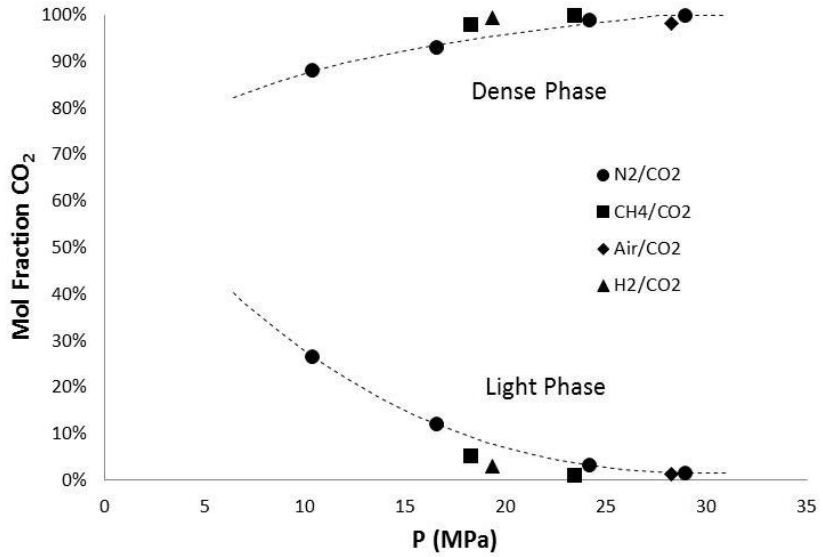

Figure 6.12. Comparison of the separation of the four systems of investigated as a function of pressure. T = 23°C, $z_i = 0.5$.

6.13 CONCLUSIONS

Fluid mixtures of nitrogen and carbon dioxide at temperatures of -5° and 23°C and pressures up to 31 MPa were explored using a HEPS. The fluid mixture was shown to be a non-homogeneous supercritical fluid with density driven concentration gradients. This density-driven concentration gradient forms the basis for a separation of nitrogen and carbon dioxide.

Increasing pressure and decreasing temperature increased the effectiveness of the N_2/CO_2 separation while consequently making the concentration gradient less pronounced. The rate of approach to equilibrium is quantified and found to decrease with increasing pressure. The separation of other binary systems including CO_2/Air, CO_2/CH_4 and CO_2/H_2 fluid mixtures were also explored in a HEPS and found to have similar trends as the CO_2/N_2 system. An effective separation of dense CO_2 with a supercritical fluid via a concentration gradient has applications in several continuous processes in gasification or refinery operations.

7. Development of Fluid Power Feeder for Viscous Biomass Slurries

One of the largest delays with the implementation of SCWG technology on a large scale is the lack a reliable feeding mechanism for a variety of biomass and waste feeds. Pumping solids and viscous slurries from ambient to very high pressure environments is a big engineering challenge. With the help of biological engineering senior design students, a novel feeder was developed to meet this need. A schematic of the design is shown in Figure 7.1.

The feeder uses a high pressure feeding chamber with a piston driven by fluid power to feed biomass slurries up to and even exceeding 50% solids content into the mixing tee in the SCWG apparatus for gasification (see Figure 3.1 in section 3.1). This fluid powered feeding chamber has proven capable of feeding a variety of slurries up to pressures of 35 MPa (5000 psi). A report from the CRC on SCWG of algae better details the capabilities of the fluid powered feeding chamber (Miller 2012).

In the design schematic, a screw auger attached to a hopper is used to reload the high pressure feeding chamber after emptying. While the design itself is reliable, the screw auger has not yet been reduced to daily operation in our lab. The screw auger works like an extrusion system. On a laboratory scale, the hopper and screw auger system proved capable of pumping slurries up to 30% solids content, however it was not able to reliably pump very viscous slurries. An upscale commercial extruder would be capable of feeder such slurries at pressures sufficient to load the high pressure chamber, but financial resources were not available to incorporate such a commercial design. During operation, the screw auger would pump slurries at a pressure of 100 – 200 psi for loading while the high pressure chamber would operate at up to 5000 psi.

It is important to note that the schematic in Figure 7.1 only shows one node of the biomass slurry feeder design. This single node operates semi-continuously as feeding has to be intermittently stopped to reload the feeding chamber. Adding a second identical node to the

design would make the design fully continuous: one chamber feeds while the other reloads. Fully continuous operation is important for commercialization of SCWG technology. Unfortunately, the funds and resources were not available to completely build and test this dual node biomass slurry feeder, however the design principles are sound and such a feeder would work well, especially after upscale.

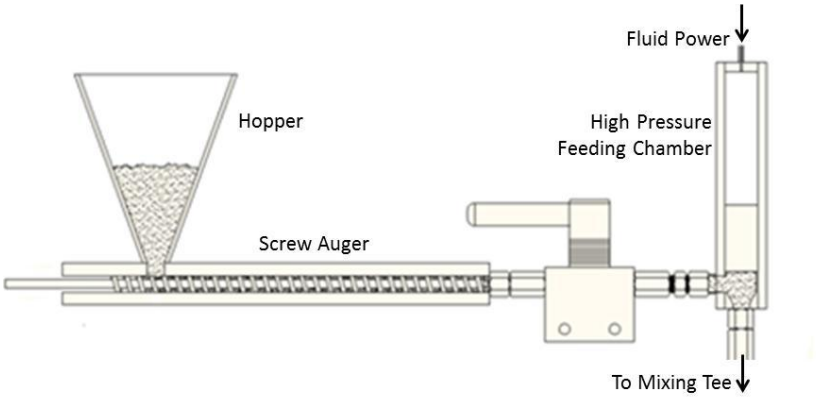

Figure 7.1. Schematic of the continuous, dual node feeder for biomass solids and slurries.

8. Mass & Energy Balances of Upgraded Continuous Apparatus

8.1 MASS & ENERGY BALANCE CALCULATIONS AND RESULTS

To fully describe the continuous SCW apparatus when used as for gasification, a mass and energy balance was performed. The experiments detailed above (Hendry 2011; Hendry 2012) provide good experimental results to act as a basis for a mass and energy balance. Additional results come from other reports from the CRC (Miller 2012; Venkitasamy 2012; Venkitasamy 2011). Figure 8.1 presents a schematic of the continuous SCW gasification apparatus and labels the different streams used a basis for the corresponding calculations. The streams of interest include: (A) feed stream, (B) recycle/preheat stream, (C) liquid product stream, (C') liquid waste and solids stream, and (D) vapor product stream. In order to do a mass and energy balance, a reference set of conditions was chosen and variables were later changed. The pressure of the system is 28 MPa (4060 psi). The temperature of the furnace and preheat stream is 700°C. The temperature profile of the fluid in the reactor is dependent on the preheat temperature and the ratio of flow rates of the preheat stream to the feed stream. The temperature of the HEPS is 350°C.

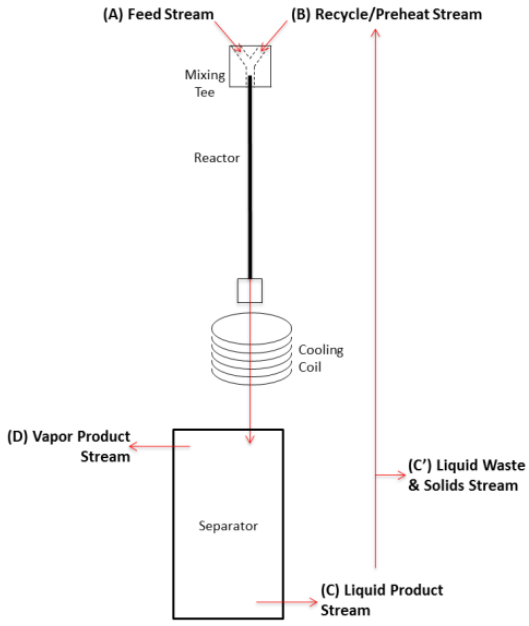

Figure 8.1. Schematic of basis for mass and energy balance for continuous SCW gasification apparatus.

The feed stream (A) is the stream where the carbon source is loaded into the mixing tee. If the feed is water soluble model compound (such as glucose or alcohol), then the feed can be loaded using positive displacement pumps. If the feed is not soluble but instead creates a solid slurry when mixed with water (such as algae or corn meal), then the feed can be feed using the fluid powered feeding chamber (as described in section 7). For the initial assessment the feed stream is assumed to be a slurry of green algae.

The recycle/preheat stream (B) is an improvement over the apparatus used in the experiments above because it allows for recycling of water leading to less water usage as well as the opportunity for heat recovery. The preheat stream will mix with the feed stream in the mixing tee as described above. The source of water in the preheat stream will come from the recycle stream, which is assumed to be pure water after the liquid and solids waste stream (C') is removed. The pressurized, subcritical water leaving the separator will contain solids, nitrogen, phosphorus, sulfur, and CO_2. The apparatus is operated at conditions leading to high gasification efficiencies (>98%), so the amount of ungasified solids, ammonia (nitrogen), phosphates (phosphorus), and sulfates (sulfur) will be small and use in applications such as fertilizers. Experimental results from the CRC and literature results (Wiebe 1940; Sabirzyano 2003) show that CO_2 had a saturated liquid phase solubility mole fraction of about 3% at 20° and 28 MPa. There was a very small variation in this value based on variation in the vapor phase product. The amount of dissolved CO_2 in the water in the HEPS at 350° is not known, but is expected to be negligible.

Despite the fact that the liquid stream leaving the HEPS has small amounts of other compounds, it was assumed to be all liquid during estimation of thermodynamic quantities. Values for H, ρ are taken as liquid values from steam tables. The mixing tee temperature as a

function of recyle:feed ratio is shown in Figure 8.2. The data in the figure come from experimental measurement and are confirmed with calculations of heat effects and phase change. It is known from previous experiments and literature sources (Hendry 2011; Hendry 2012; Kruse 2008) that highest gasification efficiencies occur when the temperature of the mixing tee is greater than the critical temperature. From Figure 8.2, the mass flow rate of the recycle stream must be at least 25% higher (50% for practical operation) than that of the feed stream in order to maintain a mixing tee temperature greater than T_c.

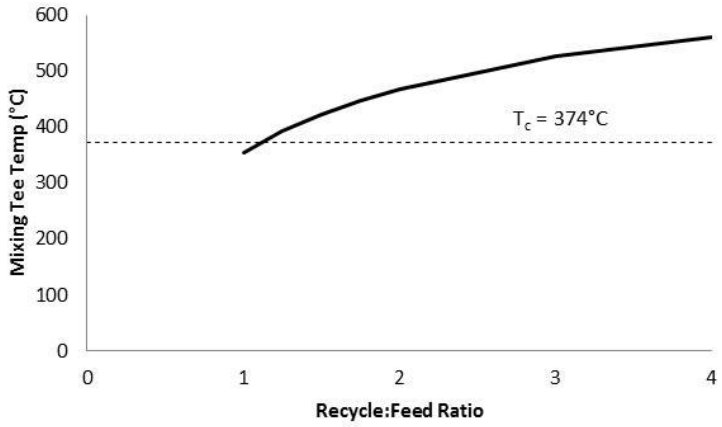

Figure 8.2. Relationship of mixing tee temperature to the flow ratio of recycle stream to the feed stream.

The work done to pump the fluid is approximated by enthalpy values of water using a 1 MPa pressure difference (27 to 28 MPa). It turns out that the work term is almost negligible compared to heat input in the energy balance. Also, it is assumed that none of the water splits during gasification. In reality, experiments from our lab show that at 700° water splits at less than 1%. However, this will not affect operation because additional water is constantly entering the system with the wet biomass slurry.

The vapor product stream (D) is a clean, dry mixture of product vapors that leaves the HEPS at 350° and 28 MPa. The energy content of the vapor product is conservatively calculated with the low heating value (LHV). At the given conditions, experimental results (Miller 2012)

show that GE is close to 100%, so the mass flow rate of vapor leaving is almost equal to the mass flow rate of carbon entering the mixing tee at steady state. There is no work done on the vapor effluent, as it will be stored at high pressure, and there is no heat change ($Q_{vap} = W_{vap} = 0$). The vapor mixture can be treated as an ideal mixture.

The results of the energy balance are presented in Figure 8.3a. Representative conditions for Figure 8.3a include a gasification temperature of 700°, a slurry concentration of 40%, a preheat water to slurry flow rate ratio of 2:1 (giving a mixing tee concentration of 13 wt%). The energy balance in Figure 8.3a also includes the amount of heat input required to achieve full gasification. The heat input required is known from results from our lab estimating the heat of gasification for each biomass species (Venkitasamy 2011). The required heat input will decrease with the addition of water and heat recycle. In Figure 8.3a, the amount heat input is shown for no heat recycle as a control for comparison with 25% and 50% heat recycle. Below the heat input in the figure is the amount of work required which is at least an order of magnitude less that the energy required for heat input.

Better understanding of the relationship between heat recycle, recycle to feed ratio, and heat requirements are presented in Figure 8.3b, which shows the rate of heat input as a function of slurry flow rate at recycle to feed flow rate ratios of 2:1, 3:1, and 4:1 and heat recovery efficiencies of 0%, 25%, and 50%. High water to feed ratios (3:1 or 4:1) will raise mixing tee temperature (see Figure 8.2) resulting in better gasification and will present more opportunity for heat recovery. However, such high water to feed ratios will also require much more heat input, thus diminishing the energy balance. Results of SCWG in our continuous reactor have shown that flow rate ratios of 2:1 are sufficient for full gasification. Therefore, for practical operation and a maximum energy balance, a water to feed ratio of between 1.5:1 and 2:1 is optimal for the largest range of biomass feeds.

The energy balance in Figure 8.3a also includes the rate of energy production, expressed as a range bounded above by algae and below by rice straw. Insight into the rate of energy production for different biomass species is presented in Figure 8.3c, which shows the energy production profile based on different types of feed materials. It is known that all biomass species and model compounds gasify to form a vapor product with the same components: H_2, CH_4, CO, CO_2, and C_2H_6 with trace amounts of other species. However, due to differences in the compositional makeup of different biomass species, the vapor product components will occur in different ratios, thus affecting the energy content of the product mixture. The compositions of the vapor product of all the feeds in Figure 8.3c are known from experiments with the batch reactor in our lab at the same conditions (Venkitasamy 2011). Also, the maximum achievable gasification efficiency is different for each biomass species based on the ash content. Ash is a component in the proximate analysis of each species along with moisture, volatile matter, and fixed carbon. Variations in moisture are accounted for by making slurry feeds with the same moisture content (60%) for each experiment. Volatile matter and fixed carbon components gasify fully at $T \geq 700°$. Ash does not gasify and limits the maximum gasification efficiency of each species. The ash content of the feed compounds used in Figure 8.3b on a dry basis are: Algae (2.5%), Sawdust (.5%), Corn Cob (1.4%), Glucose (0%), Sorghum Stover (5.9%), Rice Straw (19%), and Hog Waste (31%).

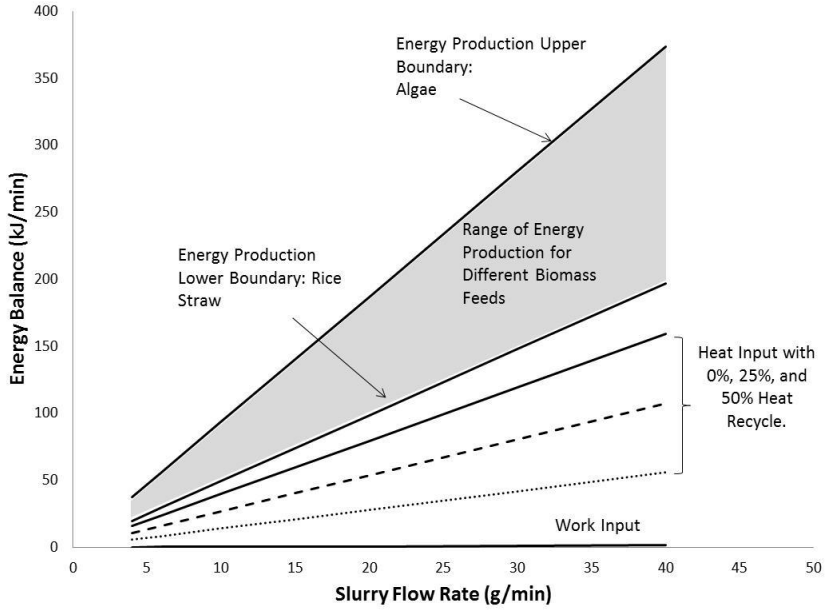

Figure 8.3a. Energy balance on continuous SCW gasification apparatus.

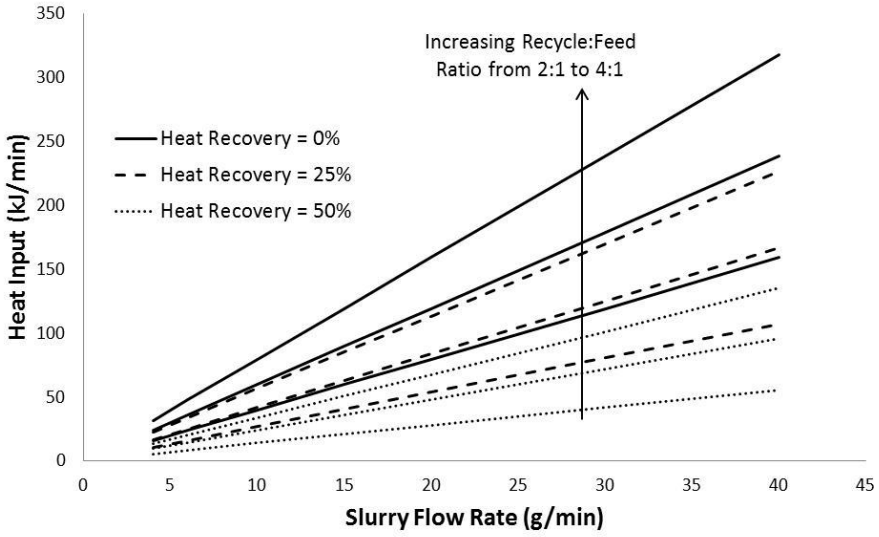

Figure 8.3b. Rate of heat input as a function of slurry flow rate at recycle to feed flow rate ratios of 2:1, 3:1, and 4:1 and heat recovery efficiencies of 0%, 25%, and 50%.

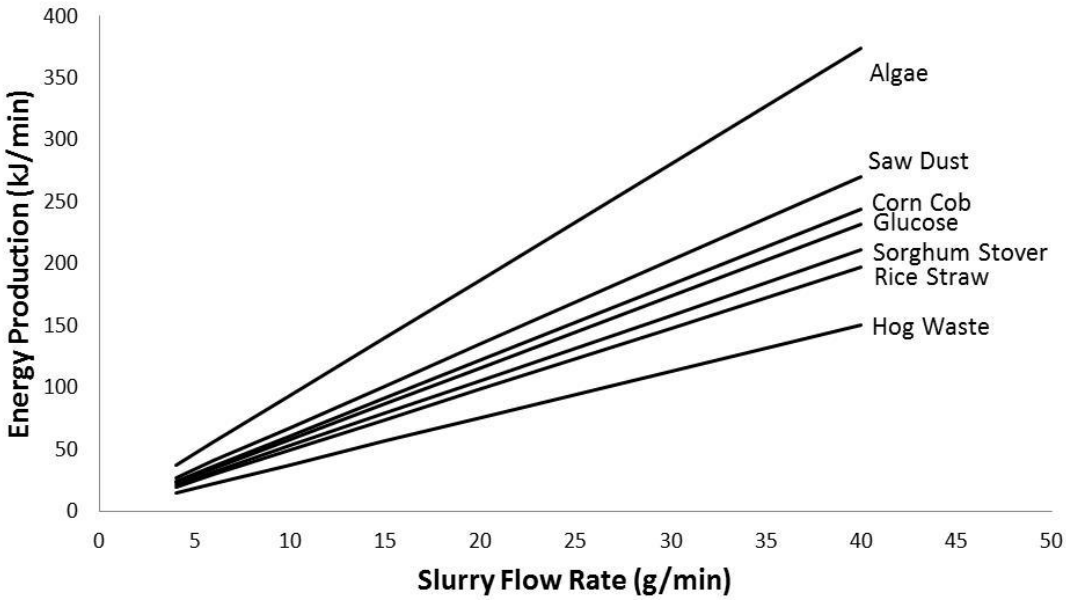

Figure 8.3c. Rate of energy production for 5 biomass species, 1 model compound, and 1 waste product as a function of slurry flow rate at a slurry concentration of 40 wt% dry feed.

8.2 *NEXT GENERATION SCWG APPARATUS*

The results of the SCWG experimental designs in sections 4 and 5, the high pressure separations in section 6, the biomass solid slurry feeder in section 7, and the mass and energy balance in section 8.1 give motivation to continue to improve the first generation SCWG apparatus (see Figure 3.1 in section 3.1). The next generation continuous SCWG apparatus will still operate on a laboratory scale, but will have several significant design features above the original apparatus that have never before been used during SCW thermochemical conversion:

1. Dual node feeding mechanism using fluid power capable of continuously feeding solid slurries up to and above 50% solids content at flow rates capable of achieving plug flow (i.e. turbulent flow) during conversion.
2. A second high pressure separation step capable of separating dense phase CO_2 from light phase fuel gases (H_2, CH_4) for carbon capture and increased energy density of vapor product.
3. Heat exchange between the cooling coil and the recycle water stream for enhanced energy balances.

The schematic of this improved SCWG apparatus is shown in Figure 8.4. The schematic details the conditions at each location in the apparatus during steady state operation as well as the products and intermediates.

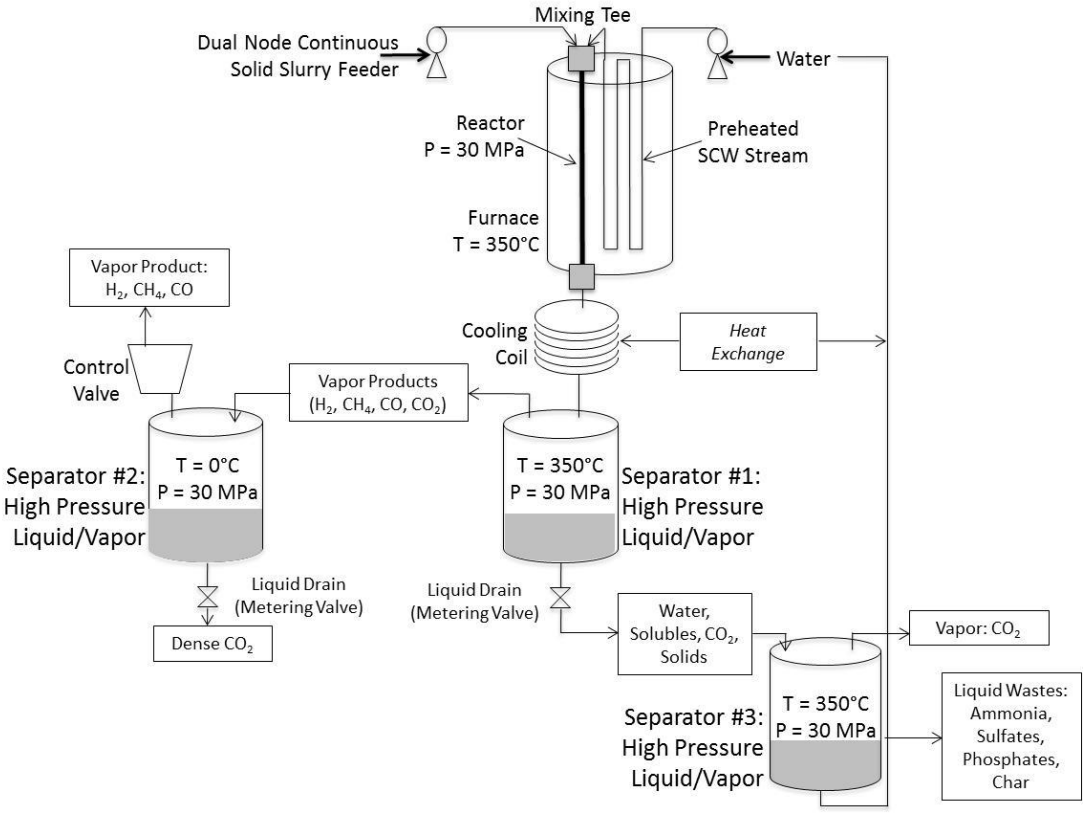

Figure 8.4. Schematic of next generation continuous SCWG apparatus in the CRC.

9. Conclusions

Based on the experiments and results detailed in sections above and supplemented with literature sources, the following conclusions can be drawn. These conclusions are noteworthy and emphasized in this section of the dissertation because they increase the amount of scientific knowledge previously available.

C_1: A well designed SCWG continuous apparatus such as the one in the CRC heats the feed stream nearly instantly to a supercritical fluid. Fast heating rate is essential for achieving both high gasification efficiencies and high gasification rates. The apparatus in the CRC is the only such continuous gasification apparatus reported in the literature capable of combining high efficiencies and rates.

C_2: In SCWG, higher feed concentrations, higher temperatures, and faster residence times lead to the highest gasification rates, but not necessarily the highest efficiencies or yields.

C_3: Temperature has perhaps the largest effect of any process variable on SCWG. High temperatures ($T > 700°C$) are capable of complete gasification even at residence times previously thought too short to obtain full gasification ($\tau < 6$ s) and without the need for catalysts.

C_4: Eliminating gradients in temperature and concentration during SCWG occurs when turbulent flow (plug flow) is achieved in the SCWG reactor, and produced gasification rates as high as 107 g/L-s which is over an order of magnitude higher than other reported reactor apparatuses. Overcoming radial transport limitations is necessary for measuring intrinsic rate data of the thermochemical reaction. Such analysis of intrinsic data, while standard in chemical engineering, was previously never applied to SCWG.

C_5: The vapor product composition of SCWG is highly dependent on the average oxidation state of the carbon in the feed which is a representative way to express feed composition.

C_6: Supercritical fluid processing leads to clean, efficient separations including opportunities for enhanced separations for carbon capture. Such separations can separate dense phase carbon dioxide from light phase fuel gases (H_2, CH_4) at sufficient pressures (P > 25 MPa) and relatively low temperatures (T < 25°C).

C_7: A novel feeding mechanism including fluid power has proved capable of feeding a variety of biomass slurries with solids contents up to 50% at high flow rates into the high pressure SCWG reaction environment. The design is also amenable to scale up to pilot scale with possibly even better performance than on a laboratory scale.

C_8: The SCWG continuous apparatus in the CRC gives opportunity for water and heat recycle with energy balance advantages.

10. Future Work

The research and results detailed in this report increase the general knowledge about processing biomass with supercritical fluids. However, the results also generate further questions for future investigation. Perhaps the first such investigation should involve a continuation of the HEPS experiments described in section 6 with the CO_2/CH_4, CO_2/H_2, and $CO_2/CH_4/H_2$ systems. After gathering important data on these binary and tertiary systems on a batch scale, focus should be put into incorporating a second HEPS into the continuous thermochemical conversion apparatus in the CRC downstream of the first HEPS for enhanced separation and carbon capture. For a visual reference, compare the original apparatus in Figure 3.1 in section 3.1 to the improved apparatus in Figure 8.4 in section 8.2.

After incorporating a second HEPS into the SCWG apparatus in the CRC, an investigation into further improving the apparatus by integrating water and heat recycle as described in section 8. Experiments would be performed and results should verify the mass and energy

balances and corresponding calculations in section 8. After these investigation have been successfully undertaken, the continuous apparatus will be ready for upscale into a pilot sized apparatus. The first part of the up-scaled apparatus to be designed should be the feeding mechanism, which is one the few parts that is expected to work better at large scale than at small scale (see section 7 for a description of the feeder). Although it will require much work and funding, a successful pilot sized continuous SCWG apparatus would bring the technology close to commercialization.

Vita

Doug was born and grew up in Chesterfield, MO and graduated from Parkway West High School in 2005. He then attended Mizzou and in 2009 earned a B.S. in Biological Engineering with an emphasis in bioprocess engineering. He also earned a minor in mathematics. As an undergraduate he worked for both the MU Learning Center and MU Residential Life. At the learning center, Doug taught/tutored chemistry, physics, and biology at the 3000 and 4000 level. At Residential Life, he worked as a Peer Advisor. Part of his responsibilities as a PA was to teach an engineering class in research methods. Also as an undergraduate, Doug spent time during summers at Monsanto Co. in Creve Coeur, MO as an automation engineer. As an undergraduate, Doug was a University of Missouri Curator's Scholar, a Missouri Bright Flight Scholar, and member of Tau Beta Pi (The Engineering Honor Society).

He continued his studies as a graduate student at Mizzou and earned his Ph.D. in Chemical Engineering in 2012. As a graduate student, he developed a strong publication record in the field of biomass processing with supercritical fluids. He research was funded with a GAANN fellowship (Graduate Assistantships in Areas of National Need). As a graduate student, Doug mentored senior engineering students during their senior design project.

Outside of his academics and work, Doug enjoys several outdoor activities, especially skiing. He is an assistant scoutmaster. He earned his Eagle Scout Award in 2002.

REFERENCES

Ahrenfeldt, J., Thomsen, T.P., Henriksen, U., Clausen, L.R. 2011. Biomass gasification cogeneration – A review of state of the art technology and near future perspectives. In press at *Applied Thermal Engineering.*

Antal, M.J., Allen, S.G., Schulan, D., Xu, X. 2000. Biomass Gasification in Supercritical Water. *Ind. Eng. Chem. Res.* 39, 4040-4053

Basu, P, Mettanant, V. 2009. Biomass Gasification in Supercritical Water - A Review. *International Journal of Chemical Reactor Engineering*.

Bermejo, M.D., Cocero, M.J., 2006. Supercritical Water Oxidation: A Technical Review. *AIChE J*. 52(11), 3933-3951.

Bobleter, O., Pape, G., 1968. Der hydrothermale Abbau von Glucose. Monatshefte für Chemie/Chemical Monthly 99, 1560–1567.

Boukis, N., Diem, V., Habicht, W., Dinjus, E. 2003. Methanol reforming in supercritical water. *Ind Eng Chem Res.* 42, 728-735.

Box, G.E.P., Hunter, W.G., Hunter, J.S., 2005. Statistics for Experimenters. John Wiley & Sons, New York.

Bridgwater, A.V., Toft, A.J., Brammer, J.G. 2002. A techno-economic comparison of power production by biomass fast pyrolysis with gasification and combustion. *Renewable and Sustainable Energy Reviews*. 6(3). 181–246.

DOE Report. 2011 U.S. Billion-Ton Update: Biomass Supply for a Bioenergy and Bioproducts Industry.

Enerkem, 2010. Enerkem Announces Construction Start of World's First Municipal Waste-to-Biofuels Facility in Edmonton, Alberta. Press Release. Edmonton, Canada. August 2010.

Faaij, A.P.C. 2006. Bio-energy in Europe: changing technology choices. *Energy Policy* 34, 322-42.

Fogler, H.S., 2004. Elements of Chemical Reaction Engineering. Fourth Edition. Pearson Education. New Jersey.

Guo, Y.; Wang, S.Z.; Xu, D.H.; Gong, Y.M.; Ma, H.H.; Tang, X.Y. 2010. Review of catalytic supercritical water gasification for hydrogen production from biomass. *Renewable and Sustainable Energy Reviews* 14, 334-343.

Hao, X.H., Guo, L.J., Mao, X., Zhang, X.M., Chen, X.J., 2003. Hydrogen production from glucose used as a model compound of biomass gasified in supercritical water. *Int J of Hydrogen Energy* 28(1), 55-64.

Hendry, D, Venkitasamy, C, Wilkinson, N, Jacoby, W. 2011. **Exploration of the effect of process variables on the production of high-value fuel gas from glucose via supercritical water gasification.** *Bioresource Technology*. 102. 3480–3487.

Hendry, D, Miller, A, Jacoby, W. **Turbulent Operation of a Continuous Reactor for Gasification of Alcohols in Supercritical Water.** *Ind & Engr Chem Res*. In Press, 2012.

Hendry, D, Venkitasamy, C, Wilkinson, N, Jacoby, W. **Exploration of High Pressure Separations of Supercritical Nitrogen and Carbon Dioxide.** In review at *Ind & Engr Chem Res.*

Hong, G.T., Spritzer, M.H., 2002. Supercritical Water Partial Oxidation. Proceedings of the 2002 U.S. DOE Hydrogen Program Review, National Renewable energy Laboratory, San Diego. pp. 18.

Johnston, B., Mayo, M.C., Khare, A., 2005. Hydrogen: the energy source for the 21st century. *Technovation* 25, 569-585.

Kersten, S.R.A., Potic, B., Prins, W., VanSwaaij, W.P.M., 2006. Gasification of model compounds and wood in hot compressed water. *Ind. Eng. Chem. Res.* 45, 4169-4177.

Kruse, A. 2008. Review: Supercritical water gasification. *Biofuels, Bioprod. Bioref.* 2, 415–437.

Kruse, A., Sinag, A., Schwarzkopf, V., 2004. Key compounds of the hydropyrolysis of glucose in supercritical water in the presence of K_2CO_3. *Ind. Eng. Chem. Res.* 42, 3516–3521.

Kumar, A., Jones, D.D., Hanna, M.A., 2009. Thermochemical Biomass Gasification: A review of the current status of the technology. *Energies* 2, 556-581.

Lee, I.G., Kim, M.S. Ihm, S.K., 2002. Gasification of Glucose in Supercritical Water. *Ind. Eng. Chem. Res.* 41, 1182-1188.

Li, H. 2008. Thermodynamic Properties of CO2 Mixtures and Their Applications in Advanced Power Cycles with CO_2 Capture Processes. ISBN 978-91-7415-091-9.

Loppinet-Serani, A., Aymonier, C., Cansell, F. 2008. Current and Foreseeable Applications of Supercritical Water for Energy and the Environment. *Chem Sus Chem* 1, 486–503.

Lu, Y, Guo, L, Zhang, X, Yan, Q. 2007. Thermodynamic modeling and analysis of biomass gasification for hydrogen production in supercritical water. *Chemical Engineering Journal* 131, 233–244.

Matsumura,Y., 2003. Evaluation of supercritical water gasification and biomethanation for wet biomass utilization in Japan. *Energy Conversion and Management* 43, 1301-1310.

Matsumura, Y., Minowa, T., Potic, B., Kersten, S.R.A., Prins, W., van Swaaij, W.P.M., van de Beld, B., Elliott, D.C., Neuenschwander, G.G., Kruse, A., Antal, M.J., 2005. Biomass Gasification in Near- and Supercritical Water: Status and Prospects. *Biomass and Bioenergy* 29(4), 269-292.

Milbrandt, A. 2005. A Geographic Perspective on the Current Biomass Resource Availability in the United States. Technical Report, NREL, Golden, Colorado, 1-62.

Miller, A., Hendry, D., Jacoby, W.A. **Gasification of Algae in Supercritical Water to Produce High-value Fuel Gas.** Accepted in *Bioresource Technology*, 2012.

Modell, M., Reid, R.C., Amin, S.I., 1978. Gasification process. US Patent 4,113,446.

Modell, M., 1982. Processing methods for the oxidation of organics in supercritical water. US Patent 4,338,199.

Modell, M., 1977. Reforming of Glucose and Wood at Critical Conditions of Water. *Mechanical Engineering* 99(10), 108-108.

Osada, M., Sato, O., Watanabe,M., Arai,K., Shirai, M., 2006. Water Density Effect on Lignin Gasification over Supported Noble Metal Catalysts in Supercritical Water. *Energy Fuels* 20, 930-935.

Puig, M., Bruno, J., Coronas, A. 2010. Review and analysis of biomass gasification models. *Renewable and Sustainable Energy Reviews* 14. 2841–2851.

Ree, F.H. 1986. Supercritical fluid phase separations: Implications for detonation properties of condensed explosives. *J. Chem. Phys.* 84, 5845.

Sabirzyanov, A.N., Shagiakhmetov, R.A., Gabitov, F.R., Tarzimanov, A.A., Gumerov, F.M., 2003. Water Solubility of Carbon Dioxide under Supercritical and Subcritical Conditions. *Theoretical Foundations of Chemical Engineering* 37(1), 51-53.

Savage, P.E. 1999. Organic Chemical Reactions in Supercritical Water. *Chem. Rev*. 99(2), 603–622.

Saxena, R.C., Seal, D., Kumar, S., Goyal, H.B. 2008. Thermo-chemical routes for hydrogen rich gas from biomass: A review. Renewable Sustainable Energy Rev 12, 1909-1927.

Schmieder, H., Abeln, J., Boukis, N., Dinjus, E., Kruse, A., Kluth, M., Petrich, G., Sadri,E., Schacht, M., 2000. Hydrothermal Gasification of Biomass and Organic Wastes. *J. Supercritical Fluids* 17(2),145-153.

Sınag, A., Gulbay,S., Uskan, B., Gullu, M. 2009. Comparative studies of intermediates produced from hydrothermal treatments of sawdust and cellulose. *J. of Supercritical Fluids* 50, 121–127.

Span, R. and Wagner, W., 1994. A New Equation of State for Carbon Dioxide Covering the Fluid Region from the Triple-Point Temperature to 1100 K at Pressures up to 800 MPa, *J. Phys. Chem. Ref. Data* 25(6):1509-1596.
Span, R., Lemmon, E.W., Jacobsen, R.T, Wagner, W., and Yokozeki, A. 1998. A Reference Quality Thermodynamic Property Formulation for Nitrogen, *Int. J. Thermophys*. 14(4):1121-1132.

Tang H and Kitagawa K, 2005. Supercritical water gasifi cation of biomass: thermodynamic analysis with direct Gibbs free energy minimization. *Chem Eng J* 106:261–267.

Venkitasamy, C., Hendry, D., Wilkinson, N., Fernando, L., Jacoby, W.A. 2011. **Investigation of thermochemical conversion of biomass in supercritical water using a batch reactor.** *Fuel* 90, 2662–2670.

Venkitasamy, C., Hendry, D., Miller, A., Jacoby, W.A. 2012. **Gasification of alcohols and algae in a supercritical water batch reactor: parameterization of rate expressions.** In press at *Fuel Processing Technology*.

Walton, M. 1960. Molecular Diffusion Rates in Supercritical Water Vapor Estimated From Viscosity Data. *American Journal of Science*. 258, 385-401.

Watanabe, M., Inomata, H., Arai, K., 2002. Catalytic hydrogen generation from biomass (glucose and cellulose) with ZrO_2 in supercritical water. *Biomass Bioenergy* 22, 405–410.

Weiss, E., Kruse, A., Ceccarelli, C., Barn, R. 2010. Influence of phenol on glucose degradation during supercritical water gasification. *Journal of Supercritical Fluids*. 53(1), 42-47.

Wiebe, R, Gaddy, VL. 1940. The Solubility of Carbon Dioxide in Water at Various Temperatures from 12 to 40° and at Pressures to 500 Atmospheres. *J. Am. Chem. Soc.* 62 (4). 815–817.

Xu, X., Matsumura, Y., Stenberg, J., Antal, Jr. M.J., 1996. Carbon-Catalyzed Gasification of Organic Feedstocks in Supercritical Water. *Ind. Eng. Chem. Res.* 35, 2522-2530.

Yan, Q., Guo, L.,Lu, Y. 2006. Thermodynamic analysis of hydrogen production from biomass gasification in supercritical water. *Energ Convers Manage* 47:1515–1528.

Yang, H., Xu, Z., Fan, M., Gupta, R., Slimane, R.B., Bland, A.E., Wright, I. 2008. Progress in carbon dioxide separation and capture: A review. *Journal of Environmental Sciences* 20. 14–27.

Yoshida, Y., Dowaki, K., Matsumura, Y., Matsuhashi, R., Li, D., Ishitani, H. 2003. Comprehensive comparison of efficiency and CO_2 emissions between biomass energy conversion technologies-position of supercritical water gasification in biomass technologies. *Biomass Bioenergy* 25:257–272.

Yoshida, T., Matsumura, Y. 2001. Gasification of Cellulose, Xylan, and Lignin Mixtures in Supercritical Water. *Ind. Eng. Chem. Res*. 40(23), 5469–5474.

Yu, D., Aihara, M., Antal, M.J. 1993. Hydrogen production by steam reforming glucose in supercritical water. *Energy Fuel* 7:574–577.